Examining the Compatibility of Collagen and a Polythiophene Derivative for the Preparation of Bioactive Platforms

Jorge Soto-Delgado,[a,b] Juan Torras,[b,*] Luis J. del Valle,[c] Francesc Estrany,[d,*] and Carlos Alemán[c,e,*]

[a] *Departamento de Ciencias Químicas, Facultad de Ciencias Exactas, Universidad Andrés Bello, Quillota 980, Viña del Mar, Chile*

[b] *Departament d'Enginyeria Química, Escola d'Enginyeria d'Igualada, Universitat Politècnica de Catalunya, Av. Pla de la Massa 8, Igualada 08700, Spain*

[c] *Departament d'Enginyeria Química, E. T. S. d'Enginyeria Industrial de Barcelona, Universitat Politècnica de Catalunya, Diagonal 647, Barcelona E-08028, Spain*

[d] *Departament d'Enginyeria Química, Escola Universitària d'Enginyeria Tècnica Industrial de Barcelona, Universitat Politècnica de Catalunya, Comte d'Urgell 187, 08036 Barcelona, Spain*

[e] *Center for Research in Nano-Engineering, Universitat Politècnica de Catalunya, Campus Sud, Edifici C', C/Pasqual i Vila s/n, Barcelona E-08028, Spain*

[*] juan.torras@upc.edu, francesc.estrany@upc.edu and carlos.aleman@upc.edu

ABSTRACT

Fundamental characteristics of bioactive platforms based on biocomposites of poly(3,4-ethylenedioxythiophene) (PEDOT) and collagen, named P(EDOT:CLG), have been examined using a experimental-computational approach. The protein affects both the morphology and electrochemical activity of PEDOT. Specifically, P(EDOT:CLG) show spherical-like nodules that has been attributed to the collagen rods aggregates organized in phases separated from that of PEDOT. This phase separation results in a reduction of the ability to exchange charge reversibly, even though collagen stabilizes the PEDOT matrix from electrochemical degradation. On the other hand, viability assays indicate that the bioactivity of P(EDOT:CLG) is significantly higher than that of PEDOT in terms of cellular adhesion and proliferation. Thus, the biocomposite promotes the formation of 3D biostructures formed by the superposition of cellular monolayers, mimiking the growing of biological tissues. In order to gain microscopic information about the formation of specific interactions between PEDOT and collagen molecules in the biocomposite, quantum mechanical calculations on complexes formed by their building blocks have been performed in different environments (*i.e.* vacuum, chloroform and aqueous solution). Results evidence the important role played by non-conventional C–H···O hydrogen bonds, which is consistent with previous findings on complexes involving DNA and dopamine. The environment affects considerably the binding energy, which decreases with increasing polarity of the environment. However, in all environment the repeat units of PEDOT form stronger interactions with L-hydroxyproline than with L-proline. On the other hand, intermolecular interaction patterns predicted using implicit and explicit solvation models present a very remarkable agreement and have been identified by visualizing the reduced electron density gradient.

INTRODUCTION

The biocompatibility and electrochemical behavior of coatings made of conducting polymers (CP)s, which have been shown to improve the charge transfer characteristics of conventional metal electrodes, are currently used in many biomedical and biotechnological applications.[1] For example, CP coatings and films have been used to fabricate active surfaces for the selective adsorption of proteins,[2,3] polymeric 2D- and 3D scaffolds for tissue engineering,[4-8] bioactive functionalized platforms[9-11] and bioelectrodes.[12,13] Combination of collagen, which is the major structural protein in animals, with synthetic polymers is a good approach for the fabrication of composite scaffolds for tissue engineering.[14-18] Thus, collagen improves the biological activity of the synthetic polymers due to its excellent biocompatibility, biodegradability and affinity towards cells. In spite of this, the number of studies devoted to fabricate bioactive platforms for tissue engineering based on the combination of collagen with CPs is, unfortunately, very scarce yet.[19-23] Thus, such studies are limited to the encapsulation of polypyrrole into collagen fibers,[19] the preparation of patterned platforms by inkjet printing polypyrrole and collagen lines on polyarate films,[20] the dispersion of polyaniline nanofibers in a collagen matrix,[21] and the preparation of CP-collagen composites using polypyrrole and polythiophene derivatives.[21-23]

Poly(3,4-ethylenedioxythiophene), hereafter abbreviated PEDOT (Scheme 1), is one of the most important CPs due to its high electrical conductivity (up to 500 S/cm), excellent electrochemical properties and biocompatibility, and fast doping-dedoping processes.[24-28] By this reason, most of the our developments in bioactive platforms for tissue engineering applications has been focused on the combination of PEDOT with peptides[10,29,30] and proteins.[12,31] More specifically, our research in PEDOT-protein composites for bioactive platforms has been focused on the use of proteins with bactericidal activity rather on structural proteins, like collagen.[12,31]

Interestingly, PEDOT chains adopt a planar all-*anti* conformation, even in the neutral state, rather than the typical *anti-gauche* conformation observed in conventional substituted polythiophenes. This conformational behavior has been explained in terms of a combination of electronic and geometric effects.[32] On the other hand, PEDOT prepared by anodic polymerization using perchlorate as dopant agent and supporting electrolyte, as in this work, is obtained in the oxidized state, $[(EDOT^{+0.5})_n(ClO_4^-)_{0.5n}]$, where each monomeric unit incorporated into the polymer chain has a charge of +0.5.[33]

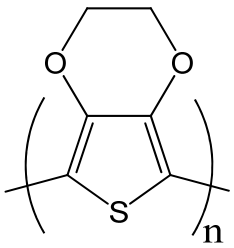

Scheme 1: Chemical structure of PEDOT

Development of new synthetic cellular matrices requires previous characterization of the biomaterials used for their fabrication as well as of the microscopic interactions that facilitate the compatibility between the different components used for their preparation. Thinking in a new family of bioactive platforms based on PEDOT-collagen biocomposites (hereafter denoted P(EDOT:CLG), in this work we used an experimental-computational approach that was proven to be successful for the development of advanced functional materials.[34,35] First, the P(EDOT:CLG) has been prepared and characterized as bioactive matrix for cell adhesion and proliferation. After such experimental characterization, specific interactions between the building

blocks of the two components of this biocomposite have been investigated using ab initio quantum mechanical (QM) calculations and hybrid quantum mechanical/molecular mechanical-molecular dynamics (QM/MM-MD) simulations. In order to examine the influence of the medium polarity in the strength of the specific interactions between the two species, QM calculations have been conducted in vaccuo and in different solvents, which were represented using a simple Self Consistent Reaction Field (SCRF) procedure. On the other hand, QM/MM-MD simulations were carried out in presence of explicit solvent molecules, allowing to consider the influence of the first solvation shell, the local solvent anisotropies and the solvent configurational sampling into the specific interactions between PEDOT and collagen building bonds.

METHODS

Materials

3,4-ethylenedioxythiophene (EDOT) monomer was purchased from Aldrich and used as received. Anhydrous $LiClO_4$, analytical from Aldrich, analytical reagent grade, was stored in an oven at 80 ºC before use in the electrochemical trials. Type-I collagen from calf skin (0.1%, $1 mg \cdot mL^{-1}$, in 0.1 M acetic acid) was purchase from Sigma Aldrich (Spain).

Synthesis

The CP and the different P(EDOT:CLG) biocomposites prepared in this work were produced by chronoamperometry (CA) under a constant potential of 1.10 V with a PAR 273A potentiostat-galvanostat connected to a computer and controlled by the PAR M270 software. Steel AISI 316 sheets of 4 cm^2 were used as working and counter electrodes while the reference electrode was

an Ag|AgCl electrode containing a KCl saturated aqueous solution (E^{o} = 0.222 V at 25 ºC). Electrochemical experiments were conducted in a three-electrode two-compartment cell under nitrogen atmosphere (99.995% in purity) at 25 ºC. The generation medium consisted on a 10 mM EDOT solution in distilled water containing 0.1 M $LiClO_4$ as supporting electrolyte. The anodic compartment was filled with 40 mL of the generation medium while a volume of 10 mL of electrolyte solution was placed in the cathodic compartment. The polymerization time (θ) was fixed at of 300 s in all cases. Four P(EDOT:CLG) biocomposites were prepared by adding different concentrations of collagen to the generation medium. The two biocomposites produced considering very low concentrations of collagen in the reaction medium (< 1 wt. %, referred to that of the EDOT monomer) provided results practically identical to the individual CP and, therefore, description of their properties have been omitted. The collagen concentrations in the reaction medium used to obtain the other two biocomposites were 4 and 16 wt. %, which correspond to 1:18 and 1:4.5 EDOT:collagen ratios, respectively. The resulting composites have been denoted 18-P(EDOT:CLG) and 4.5-P(EDOT:CLG), respectively.

FTIR spectroscopy

FTIR spectra were recorded on a FTIR 4100 Jasco spectrophotometer with a resolution of 4 cm^{-1} in the absorbance mode. Samples were placed in an attenuated total reflection accessory with thermal control and a diamond crystal (Golden Gate Heated Single Reflection Diamond ATR).

Scanning electron microscopy (SEM)

SEM studies were performed to examine the effect of the protein on the surface morphology. Dried samples were placed in a Focussed Ion Beam Zeiss Neon 40 scanning electron microscope operating at 3 kV, equipped with an EDX spectroscopy system

Electrochemical characterization

The electrochemical response of the prepared biocomposites was determined in water using cyclic voltammetry (CV). The initial and final potentials were -0.50 V, while a reversal potential of 1.40 V was considered. A scan rate of 50 $mV \cdot s^{-1}$ was used in all cases.

Cell adhesion and proliferation tests

In vitro adhesion and proliferation assays were performed using two different cellular lines of adherent growth: (i) cells HEp-2 (human line derived from an epidermoid carcinoma of larynx); and (ii) cells Du-145 (human line derived from a prostate carcinoma). HEp-2 and Du-145 have an epithelial morphology. Tissue culture polystyrene (TCPS) plate has been used as control substrate.

Cells were plated in 25 cm^2 tissue flasks and grown in Dulbecco's Modified Eagle's Medium (DMEM) supplemented with 10% fetal bovine serum (FBS), penicillin G (100 U/ml) and streptomycin (100 mg/mL). Cultures were performed at 37 °C and humid atmosphere with 95% air (5% carbon dioxide). Passage 2 cultures were used for experiments. Cellular confluent cultures were dissociated with 0.05% trypsin and 0.02% EDTA in phosphate buffer saline (PBS) solution, harvested by centrifugation, and counted in Neubauer camera using 0.4% trypan blue.

Adhesion and proliferation assays were performed seeding 5×10^4 and 2×10^4 cells, respectively, from an appropriate cell suspension concentration with viability >95%. PEDOT and

P(EDOT:CLG) films electrodeposited on 1 cm^2 steel sheets were placed in 24-well plates, and subsequently sterilized by UV-radiation during 15 min in the laminar flow cabinet. Next, cells were seeded by a slowly pipette of the cell suspension onto the top surface of each sample, covering 80-90% of the sample's surface. In order to avoid a reduction of the seeding efficiency, no contact between cell suspensions and the sides of the wells was allowed. The plates were placed with care into an incubator, avoiding agitation. After 1 h, fresh medium (1 mL) was added into each well and the plate was returned to the incubator. Cultures to evaluate cellular adhesion and proliferation were incubated during 24 h and 7 days, respectively. All experiments were repeated at least three times.

To evaluate the cell number in the samples, the medium of each well was changed by fresh medium supplemented with MTT [3-(4,5-dimethylthiazol-2-yl)-2,5-diphenyltetrazolium; 5 mg/mL] and the plate returned to the incubator for 3 h. After this, the medium of each well was removed and the samples recoveries were placed in wells of a clean plate. The MTT reaction in the viable cells was determined by dissolving the formazan crystals in 1 mL of DMSO/methanol/water (70%/20%/10%, % in vol.). Then, the absorbance at 540 nm was read in a microplate reader (Biochrom Ltd., UK). Analyses were carried out using the cell adherence density in each sample in comparison to the control (%, relative of control).

To evaluate the cellular morphology, samples incubated with cells were fixed in 1 mL of 2.5% paraformaldehyde in PBS during 24 h at 4 ºC. Then, samples were progressively dehydrated using alcohols of 30º, 40º, 50º, 70º, 90º, 95º, and 100º for 30 min at 4 ºC in each one. Finally, samples were coated by carbon sputtering for the observation in the scanning electronic microscope.

Quantum mechanical (QM) calculations

Ab initio QM calculations were used to examine the strength of the specific interactions between PEDOT and collagen. For the selection of appropriated models, it should be noted that the excellent behavior of CP-biomolecule composites as bioactive platforms is essentially due to the ability of CPs to exchange ions with cells and to the favorable biomolecule···cell interactions.[10,28,31] In contrast, properties related with electron delocalization along polymer chains are not relevant for for bioactivity. Accordingly, selection of small model compounds was considered appropriate for understanding the specific interactions between the components of P(EDOT:CLG). More specifically, complexes involving the main building blocks of these PEDOT and collagen were constructed for their subsequent study in different environments. In a recent work we proved that the selection of EDOT (*i.e.* the repeat unit of the PEDOT) is enough to describe specific interactions in PEDOT···biomolecule complexes. Thus, we observed that the specific interactions between PEDOT and DNA can be modeled using a single EDOT unit and the nucleotide bases.[36] On the other hand, L-proline (Pro) or L-hydroxyproline (Hyp) have been selected because they are the most relevant constituents of collagen. Thus, the most common motifs in the amino acid sequence of collagen are Gly-Pro-X and Gly-X-Hyp, where X is any amino acid other than Gly, Pro or Hyp. In order to mimic the protein environment at the ends of the Pro and Hyp residues, their *N*-acetyl-*N*'-methylamide derivatives, hereafter denoted Ac-L-Pro-NMe and Ac-L-Hyp-NMe (Figure 1), respectively, were considered for the calculations. Regarding to the selected model compounds, it should be noted that the EDOT monomer is not suitable to reproduce the electronic properties of PEDOT. Thus, the band gap of PEDOT determined using electrochemical and DFT methods is 1.98[37] and 1.90[38] eV, respectively, while the HOMO-LUMO transition energy of EDOT is higher than 4 eV.[39] In spite of this limitation,

EDOT captures the essential trends required for the formation of specific interactions (*i.e.* polar oxygen atoms and polarized C–H bonds to form conventional and non-conventional hydrogen bonds, respectively).

Calculations were performed using the Gaussian 09[40] computer packgage. The structures of the complexes were determined by geometry optimization in vacuum using the second-order Møller-Plesset Perturbation Theory (MP2) methodology[41] combined with the 6-31+G(d, p) basis set.[42,43] Because the dihedral angle ψ of Ac-L-Pro-NHMe and Ac-L-Hyp-NHMe (Figure 1) is rather flexible, it was constrained during geometry optimization at 163º and 152º, respectively, which are the typical values adopted by these amino acids in collagen, respectively.[44] Binding energies were corrected with the basis set superposition error (BSSE) by mean of the standard counterpoise (CP) method but incorporating the relaxation energy into correction.[45] The binding energy of the complex is defined as usual by:

$$BE_{CP} = E_{complex} - [\, E_{EDOT} + E_{AA} \,] + E_{BSSE} \qquad (1)$$

where $E_{complex}$ is the MP2 energy of the optimized complexes, and E_{EDOT} and E_{AA} are the MP2 energies of the EDOT monomer and the Ac-X-NHMe dipeptide (with X= L-Pro or L-Hyp), respectively, derived from their minimization alone.

The structures of EDOT···Ac-X-NHMe complexes were also optimized in both chloroform and water, which were described through a simple SCRF method. Vacuum geometries were used as the starting points for optimizations in such condensed environments. The dihedral angle ψ of Ac-L-Pro-NHMe and Ac-L-Hyp-NHMe was restricted during the energy minimization at the same values that in vacuum calculations. The Polarizable Continuum Model (PCM)[46,47] was used to represent the bulk solvent effect. PCM calculations were performed in the framework of the ab initio MP2 level combined with the 6-31+G(d, p) basis set and considering the dielectric

constants of chloroform (ε=4.9) and water (ε= 78.4). The binding energies in solution, which provide information about the strength of the interactions in solution, were computed using the same procedures that for the vacuum.

The energy-minimized conformations of Ac-L-Pro-NHMe and Ac-L-Hyp-NHMe have been denoted using a two-label code that specifies the backbone conformation and the puckering of the five-membered ring. The first label identifies the backbone conformation using the well-established nomenclature introduced by Perczel *et al.*[48] two decades ago. In this work the backbone of all minimized structures exhibits the ε_L (polyproline II-like) conformation because of the constraint imposed in the ψ dihedral angle. Next, the *up* or *down* puckering of the five-membered ring is indicated using the [u] and [d] labels, respectively. The puckering of the five-membered ring has been described using the classical pseudorotational parameters, which uses a very simple model based on only two parameters. Details about the calculation of the pseudorotational parameters A and P, which describe the puckering amplitude and the state of the pucker in the pseudorotation pathway, respectively, are provided in our previous studies on Pro derivatives.[49-51]

Hybrid quantum mechanical/molecular mechanical-molecular dynamics (QM/MM-MD) calculations.

In order to take into account the influence of important solvent effects (*i.e.* interactions at the first solvation shell, anisotropy and configurational entropy) as well as the dynamic hydrogen bond network, hybrid QM/MM-MD calculations were conducted. This methodology is based on an explicit solvation model to investigate the dynamics of EDOT···Ac-X-NHMe (with X= L-Pro or L-Hyp) complexes in a solvated environment. In this approach atomic motions are handled by

molecular dynamics (MD), energies and forces being calculated by dividing the system into two different parts. The EDOT···Ac-X-NHMe complex is treated at the QM level while molecular mechanics (MM) using a classical potential energy function is employed to describe the rest of the system (*i.e.* explicit solvent molecules).

In this work ecah complex was solvated by assigning a 10 Å buffer region made of 400 and 2000 chloroform and water molecules, respectively. Chloroform molecules were described using the Cieplak *et al.*[52] model while the TIP3P model[53] was employed for water molecules. Moreover, all force field parameters for Ac-L-Pro-NHMe and Ac-L-Hyp-NHMe were taken from the Generalized AMBER Force Field (GAFF)[54] libraries. Force-field parameters for EDOT, including the electrostatic ones, were explicitly derived in a previous work[55] and subsequently tested by examining PEDOT···DNA[55] and PEDOT···PEDOT[56] interactions. Charges for EDOT, which are included in the Supporting Information, were derived from the electrostatic potential (ESP charges) calculated at the UB3LYP/6-31+G(d,p) level. MD trajectories were obtained using the AMBER 12 software package.[57]

Initially, the four systems simulated using QM/MM-MD were minimized at the MM level, heated up to 298 K and, finally, equilibrated using a NPT ensemble for 0.5 ns at 1 atm and 298 K (2 fs time steps). The atomic positions of EDOT···Ac-X-NHMe complexes were restrained to the initial geometry by a force constant of 20 kcal/(mol·Å^2) in both thermalization and equilibrations steps. The SHAKE algorithm[58] was used to keep the bond lengths involving hydrogen atoms at their equilibrium distance. Atom pair distance cutoffs were applied at 10 Å to compute van der Waals interactions. Electrostatic interactions were computed using the nontruncated electrostatic potential by means of Ewald summations.[59]

Hybrid QM/MM-MD calculations were run using PUPIL interface,[60,61] which allows to link, among others, QM calculations from NWChem[62] program with MD simulations from AMBER 12[57] program. The starting structures were extracted from the last classical MD equilibration snapshot, after reach the correct solvent density, using the NWChem-PUPIL-Amber interface.[63] Subsequently, the EDOT···Ac-X-NHMe complexes were changed to a QM description while the solvent molecules remained within the MM framework. Thus, all atoms from the QM region were described by combining M06-2X functional[64] with the 6-31G basis set. It should be remarked that the M06-2X functional describes medium-range (*i.e.* ≤ 5 Å) non-covalent interactions, such as conventional (*e.g.* N–H···O and H–O···H) and non-conventional (*e.g.* C–H···O) hydrogen bonds, better than usual DFT functionals.[65] After that, the systems were allowed to relax for 0.5 ps with a production run of 2 ps (5000 steps, 0.5 fs time step) in the NVT ensemble at 298 K with the same parameters previously used for fully classical MD simulations. It should be noted that QM/MM-MD calculations are very demanding from a computational point of view and, therefore, a good compromise between computational time and observable data to be obtained should be carefully considered. The main goal in this work is not to reach perfectly equilibrated systems to extract statistical information, as in classical MD, but a sufficiently relaxed system in the QM/MM framework to examine the behavior of the formed specific interactions. Thus, 2 ps of simulation allows the system relaxation with root mean square deviations average in the last picosecond of 0.649±0.073 and 0.453±0.047 Å for the Hyp-containing complex in water and chloroform, respectively, and 1.078±0.135 and 0.560±0.131 for the Pro-containing complex in water and chloroform, respectively. Similarly to previous QM calculations, the backbone dihedral angle ψ of Ac-L-Pro-NHMe and Ac-L-Hyp-NHMe was constrained during QM/MM-MD trajectories at 163º and 152º, respectively. Periodic boundary

conditions were applied in the preparation of the NWChem input so as to wrap neighboring point charges around the quantum region. The coordinates of relaxing trajectories on the last 2 ps were saved for subsequent analyses.

Characterization of the weak Non-Covalent Interactions (NCI) on the temporally averaged complex structures was performed with the NCIPlot program.[66,67] The NCI surface enables the study of domains of the electronic density associated with weak interactions, being able to distinguish the strength and the attractive or repulsive nature of such interactions. Recently, this method has expanded to understand the reactions mechanism in enzymatic reactions using QM/MM method.[68]

RESULTS AND DISCUSSION

Preparation and characterization of P(EDOT:CLG) composites

Figure 2 compares the FTIR of PEDOT, free collagen and 4.5-P(EDOT:CLG) in the 1730-1450 cm^{-1} range. This interval corresponds to the amide I and II bands, which have been used to identify the presence of the protein in P(EDOT:CLG) biocomposites. The amide I band (1700-1600cm^{-1}) arises primarily from the C=O stretching vibration of the peptide linkages that constitute the backbone structure of proteins and is well-known to be sensitive to the conformational changes[69] The amide II band (1600-1480 cm^{-1}) is assigned to the coupling of the N–H in plane bending and the C–N stretching modes of peptide linkages.[70] Free collagen films prepared by drop-casting show the characteristic broad and intense bands centered at 1640 and 1545 cm^{-1} for amide I and amide II, respectively.[71] For 4.5-P(EDOT:CLG) these vibrations split into bands near 1647 and 1620 cm^{-1} for amide I and 1541 and 1515 cm^{-1} for amide II, suggesting the coexistence of the collagen native triple helix (1647 and 1541 cm^{-1}) and denatured collagen

(1620 and 1515 cm^{-1}).[72] These bands are also detectable in 18-P(EDOT:CLG), even though their definition is considerably poorer than for 4.5-P(EDOT:CLG) because of the low protein concentration (not shown). In contrast, those bands are undetectable PEDOT (Figure 2).

Figure 3 shows the surface morphology of PEDOT and P(EDOT:CLG) films. As it can be seen, the incorporation of collagen to the generation medium affects the typical clustered morphology of PEDOT. The most relevant difference corresponds to the apparition of spherical-like nodules, which have been attributed to collagen, at the surface of the biocomposites. The size of the nodules is larger than the fundamental structural unit of collagen, which organizes as molecular rods of ~280 nm in length and ~1.5 nm in diameter denoted tropocollagen.[73] A possible explanation to this feature is that collagen molecular rods aggregate in a phase separated from that of the polymer rather than act as soft templates during the anodic polymerization process. Thus, the surface energies of PEDOT and collagen are probably incompatible since both are positively charged systems (*i.e.* collagen involves a relative large number of positively charged amino acids and PEDOT chains contain around 0.5 positive charges per repeat unit[33]).

Cyclic voltammograms of PEDOT and P(EDOT:CLG) were recorded to evaluate the influence of the protein in the electroactivity (*i.e.* ability to exchange charge reversibly) and electrostability (*i.e.* variation of the electroactivity with consecutive oxidation-reduction cycles). The electroactivity increases with the similarity between the anodic and cathodic areas. Figure 4, which compares the voltammograms recorded for PEDOT and 4.5-P(EDOT:CLG), indicates that the protein provokes a very significant reduction in the electroactivity of the CP, affecting drastically its ability to exchange charge. This drawback is similar for 18-P(EDOT:CLG) (not shown) than for 4.5-P(EDOT:CLG). However, the reduction of the electroactivity after 15 consecutive oxidation-reduction cycles is noticeable higher for PEDOT than for the

biocomposites (grey lines in Figure 4), suggesting that the protein stabilizes the structure of the polymeric matrix in the biocomposite. More specifically, voltammograms displayed in Figure 4 are consistent with an increment in the compactness of the CP structure with increasing number of redox cycles, which makes more difficult the access and escape of the dopant ions upon oxidation and reduction, respectively, and provokes a reduction of the electroactivity. This effect is considerably less pronounced for the biocomposite than for the CP, the loss of electroactivity after 15 redox cycles being very small for the former (Figure 4b).

The abilities of 4.5-P(EDOT-CLG), 18-P(EDOT-CLG) and PEDOT substrates to cellular adhesion and proliferation were compared by considering two different cellular lines: HEp-2 and Du-145. These carcinogenic cells were selected due to their fast growth. Quantitative results of cellular adhesion assays are displayed in Figure 5a, TCPS (or culture plate) being used as control substrate. Results indicate that collagen considerably enhances the adhesion of the cells. Thus, the percentage of adhered cells was around 40-60% higher for the two P(EDOT:CLG) biocomposites than for the PEDOT and TCPS. After 7 days of culture, the cellular activity was re-evaluated. Results, which are displayed in Figure 5b, show that the number of proliferated cells per area of P(EDOT:CLG) increases with respect to the number of adhered cells per area of the same material, this incremement being more appreciable for HEp-2 cells than for Du-145 cells (*i.e.* > 20% and < 10%, respectively). The fact that such improvement is observed for the two P(EDOT:CLG) compositions while it is almost undetectable for the CP without protein indicates that enhancement of the cell affinity must be attributed to the collagen. Thus, although PEDOT is not cytotoxic[28] and is able to support cell attachment, the incorporation of collagen molecules greatly improves its cell binding abilities. On the other hand, relative viabilities determined from cell adhesion and profileration assays using 4.5-P(EDOT-CLG), 18-P(EDOT-

CLG) films are similar, differences between the two composites being unmeaning. This feature together with the low relative viabilities obtained for PEDOT indicates that, after a given threshold, the influence of the collagen concentration is not relevant for the cell behavior.

SEM micrographs displayed in Figures 6a and 6b show the characteristics of HEp-2 cells cultured onto the surface of PEDOT and 4.5-P(EDOT:CLG), respectively. In general, the spreading of the cells attached to the surface is more pronounced for the biocomposite than for PEDOT. The connection sites between the cells and the biocomposite surface consist on actin filaments known as filopodia (marked with arrows in Figure 6b). Interestingly, these filaments, which are used for local adhesion of the cell onto the substrate and, extend from the cell to the spherical-like collagen nodules. After 7 days, cultured cells colonize the biocomposite giving place to a cellular monolayer (Figure 6c), which in turn supports the adhesion of new cells facilitating the formation of more cellular monolayers (Figure 6d). The superposition of celular monolayers results in 3D biostructures, like those displayed in Figures 6e and 6f, mimiking the growing of biological tissues.

Specific interactions between building blocks

Initially, the conformational preferences of Ac-L-Pro-NHMe and Ac-L-Hyp-NHMe in different environments were explored for subsequent comparison with the geometries obtained for EDOT···Ac-L-Pro-NHMe and EDOT···Ac-L-Hyp-NHMe complexes. It is known that on the triple helix of collagen, the pyrrolidine ring Pro residue adopts a *down* (C^{γ}-*endo*) or an *up* (C^{γ}-*exo*) puckering depending on its position into the polypeptide chain.[74] On the other hand, the five-membered ring of Hyp residue usually retains the C^{γ}-*exo* puckering conformation, which is believed to be stabilized by a *gauche* effect.[75,76] This electronic effect has been attributed to the

electron-withdrawing ability of the hydroxyl group.[77,78] In order to examine properly the *gauche* effect, the ξ dihedral angle (defined as N-C^{δ}-C^{γ}-O in Figure 1, where O is the oxygen of the hydroxyl group in Hyp), which in turn is related with the pyrrolidine ring puckering, was followed. Accordingly, the ξ dihedral angle is near the *anti* conformation for the *down* puckering arrangement presents, whereas in the *up* puckering this dihedral adopts a *gauche* conformation. In addition, the dihedral angle ϕ and the pseudorotational parameters have been carefully followed to characterize the conformational preferences of Ac-L-Pro-NHMe and Ac-L-Hyp-NHMe in absence of interactions with EDOT.

Table 1 summarizes the conformational parameters for the energy-minimized conformations of Ac-L-Pro-NHMe and Ac-L-Hyp-NHMe in different environments. As it can be seen, the ε_L is the only stable backbone conformation for the two dipeptides (see Methods section), independently of both the polarity of the environment and the five-membered ring puckering, with ϕ ranging from -61º to -71º. In this backbone arrangement the pyrrolidine ring of Ac-L-Hyp-NHMe and Ac-L-Pro-NHMe exhibits envelope conformations with C^{γ} at the flap pointing to the same (*down* or C^{γ}-*endo*) or the opposite (*up* or C^{γ}-*exo*) side of the molecule where the carboxylic terminus is located. However, the variation of the relative energy between the *up* and *down* puckerings ($\Delta E^{up\text{-}down}$) with the polarity of the environment is different for each dipeptide. Thus, while $\Delta E^{up\text{-}down}$ calculated for Ac-L-Hyp-NHMe residue increases very sharply with the polarity (*i.e.* from < 0.1 kcal/mol in vacuum to 1.5 kcal/mol in aqueous solution), for Ac-L-Pro-NHMe value of $\Delta E^{up\text{-}down}$ decreases with increasing polarity. In all cases the dihedral angles ξ and ϕ tend to increase their absolute value with the polarity of the medium. Similarly, the pseudorotational parameter P decreases in absolute value with increasing polarity, even though the puckering parameters are similar for the dipeptides when the same conformations are compared.

In order to ascertain the ability of EDOT units to form specific interactions with the Pro and Hyp residues of collagen, QM calculations were performed on EDOT···Ac-L-Pro-NMe and EDOT···Ac-L-Hyp-NMe complexes. The EDOT unit was considered in the neutral (reduced) state rather than in the doped (oxidized) one. The main reason of this choice is based on the electronic structure of oxidized polyconjugated polymers, which consists on small segments of charged repeat units (*i.e.* quinoid-like structure) separated among them by segments of repeat units in the neutral state (*i.e.* benzenoid-like structure).[738,39,79] Accordingly, this choice enables us to focus the theoretical study on the participation of EDOT units in specific hydrogen bonding interactions with Pro and Hyp residues while oxidized segments would be essentially involved in non-specific electrostatic interactions with collagen.

A total of 40 starting geometries were prepared for EDOT···Ac-L-Pro-NMe and EDOT···Ac-L-Hyp-NMe complexes applying the following scheme: (*i*) the EDOT unit was combined with the dipeptides in such a way that 10 hydrogen bonded complexes were constructed using one of the oxygen atoms of the dioxane ring as interaction site; (*ii*) two different conformations were considered for the five-membered ring of each residue (*i.e. up* and *down*). Accordingly, all possible complexes stabilized by specific interaction have been considered as starting points, guarantying that the global minimum will be among the structures obtained after optimization. As was done above for the isolated dipeptides, the dihedral angle ψ was constrained at 163º and 152º during the energy minimization. Geometry optimizations at the MP2/6-31+G(d, p) level in vacuum provided a distribution of relative energies (ΔE_{vac}) from which only those complexes with a $\Delta E_{vac} \leq 3$ kcal/mol (*i.e.* 9 for EDOT···Ac-L-Pro-NMe and 9 EDOT···Ac-L-Hyp-NMe) were considered for further calculations. The optimized geometries of the selected EDOT···Ac-

L-Pro-NMe and EDOT···Ac-L-Hyp-NMe complexes are displayed in Figures 7 and 8, respectively.

Table 2 lists the ΔE_{vac} values and the binding energies ($BE_{CP,vac}$), which were estimated with the correction of the BSSE, for all the complexes optimized in vacuum. Five EDOT···Ac-L-Pro-NMe show $\Delta E_{vac} \leq$ 2 kcal/mol, three of them being exclusively stabilized through C–H···O interactions (1Pro-E, 4Pro-E and 5Pro-E). The EDOT···Ac-L-Pro-NMe complex of lowest energy in vacuum, 1Pro-E, is stabilized through a simple C–H···O=C interaction while the second complex, 2Pro-E, which is destabilized by only 0.2 kcal/mol, exhibit a N–H···π interaction between the *N*'-methylamide blocking groups and the thiophene ring in addition to the same interaction that 1Pro-E. Accordingly, the $BE_{CP,vac}$ is lower for 2Pro-E (-8.1 kcal/mol) than for 1Pro-E (-6.8 kcal/mol). On the other hand, 1Pro-E and 4-Pro-E only differ in the puckering of the pyrrolidine ring, which is consistent with their identical $BE_{CP,vac}$ values (*i.e.* both complexes are stabilized by the same C–H···O=C interaction) and the destabilization of the latter with respect to the former by 1.4 kcal/mol. The $BE_{CP,vac}$ of the remaining optimized complexes ranges from -6.9 to -5.8 kcal/mol, the predominant interactions being the C–H···O in all cases with exception of 3Pro-E that is exclusively stabilized by a N–H···O hydrogen bond. Despite of this specific interaction, 3Pro-E is destabilized by 1.1 kcal/mol with respect to 1Pro-E and its $BE_{CP,vac}$ is 2.1 kcal/mol higher than that of 2Pro-E. The pyrrolidine ring adopts the *up* puckering in 6 of the 9 complexes, the complex with lowest ΔE_{vac} (1Pro-E) and lowest $BE_{CP,vac}$ (2Pro-E) exhibiting a *down* and *up* puckering, respectively. On ther other hand, five EDOT···Ac-L-Hyp-NMe complexes present $\Delta E_{vac} \leq$ 2 kcal/mol, all them showing stabilizing C–H···O interactions while only two (1Hyp-E and 4Hyp-E) exhibit O–H···O hydrogen bonds. The $BE_{CP,vac}$ ranges from -8.8 to to -6.1 kcal/mol. The O–H···O hydrogen bond found in the 1Hyp-E

complex, which shows the lowest ΔE_{vac} and $BE_{CP,vac}$ values, involves the hydroxyl group of Hyp residue and one of the oxygen atoms of the dioxane ring. The second complex, 2Hyp-E, which is only destabilized by 1.2 kcal/mol and does not present conventional hydrogen bonds, exhibits a $BE_{CP,vac}$ value 1.4 higher than 1Hyp-E only. The pyrrolidine ring adopts the *up* puckering in 6 of the 9 complexes, the only 3 with a *down* puckering being 3Hyp-E, 8-Hyp and 9Hyp-E (*i.e.* ΔE_{vac}= 1.5, 27 and 2.7 kcal/mol, respectively.

Comparison of the $BE_{CP,vac}$ values calculated for the EDOT···Ac-L-Pro-NMe and EDOT···Ac-L-Hyp-NMe complexes indicates that the latters present the most favorable interactions, which should be attributed to the hydrogen bonding ability of the hydroxyl group contained in the Hyp residue. Despite of this, the results obtained for these two families of complexes evidence that the energetic associated to the C–H···O interaction is significantly important, as was also recently found in other recent studies involving complexes formed by biomolecules (e.g. DNA bases and neurotransmitters) and building blocks of different CPs.[36,80]

The geometries of EDOT···Ac-L-Pro-NMe and EDOT···Ac-L-Hyp-NMe complexes optimized in vacuum were used as starting points for optimizations in chloroform solution. The resulting geometries (Figures S1 and S2 in the ESI) do not show important differences with respect to those displayed in Figures 7 and 8. Comparison of the energetic parameters displayed in Table 3 with those obtained in vacuum (Table 2) indicates that chloroform probokes important changes in the relative stability of a few EDOT···Ac-L-Pro-NMe complexes. Thus 5Pro-E and 9Pro-E stabilize by 1.2 and 1.6 kcal/mol, respectively, while 2Pro-E destabilizes by 1.2 kcal/mol. For the rest of the EDOT···Ac-L-Pro-NMe and EDOT complexes the relative energies in chloroform solution (ΔE_{chl}) are very similar to the ΔE_{vac} values (*i.e.* $|\Delta E_{chl} - \Delta E_{vac}| \leq 0.4$ kcal/mol). The effect of bulk chloroform in the relative stabilities is more pronounced for EDOT···Ac-L-Hyp-

NMe complexes. Accordingly, 2Hyp-E, 4Hyp-E, 5Hyp-E, 7Hyp-E and 9-Hyp-E experiences a significant stabilization (*i.e.* from 1.1 to 2.2 kcal/mol). Moreover, 1Hyp-E, 2Hyp-E and 4Hyp-E show $\Delta E_{chl} \leq 0.1$ kcal/mol, whereas in vacuum the former was favored by 1.2 and 2.3 kcal/mol, respectively. On the other hand, the binding energy in chloroform solution ($BE_{CP,chl}$) decreases significantly with respect to the vacuum. Thus, for EDOT···Ac-L-Pro-NMe and EDOT···Ac-L-Hyp-NMe complexes the $BE_{CP,chl}$ ranges from -3.6 (6Pro-E) to -5.1 kcal/mol (2Pro-E) and from -3.8 (6Hyp-E) to -5.8 kcal/mol (1Hyp-E), respectively, wheras $BE_{CP,vac}$ varied between -5.8 (9Pro-E) and -8.1 kcal/mol (2Pro-E) and between -6.1 (9Hyp-E) and -8.8 kcal/mol (1Hyp-E). In spite of this ~2-3 kcal/mol reduction, results indicate that EDOT forms stronger complexes with Hyp than with Pro, independently of the environment.

Results obtained after geometry optimization in water of the EDOT···Ac-L-Pro-NMe and EDOT···Ac-L-Hyp-NMe complexes (Table 4) re-inforce the tendencies observed in chloroform solution. As occurred above, water does not provoke significant variations in the on the peptide conformation (Figures S3 and S4). In contrast, changes in the relative stabilities and binding energies (ΔE_{wat} and $BE_{CP,wat}$, respectively) are more marked in water than in chloroform. Accordingly, 2Pro-E, 3Pro-E and 9Pro-E are destabilized by 0.7 kcal/mol or less with respect to 1Pro-E, which is the still the most stable EDOT···Ac-L-Pro-NMe complex. Among these four low-energy complexes, 3Pro-E is the only with a N–H···O hydrogen, all the other being stabilized by C–H···O interactions (Figures S3). $BE_{CP,wat}$ values vary between -4.3 and -2.9 kcal/mol, which respresent a reduction of ~4 and ~1 kcal/mol with respect to the $BE_{CP,vac}$ and $BE_{CP,chl}$ intervals, respectively.

Changes are even more important for EDOT···Ac-L-Hyp-NMe complexes. Thus, 1Hyp-E, 2Hyp-E, 4-Hyp-E and 5-Hyp-E complexes, which are the more stable, are separated by 0.3

kcal/mol only while 7Hyp-E is destabilized by 0.8 kcal/mol with respect to the lowest energy one (5Hyp-E). Interestingly, the four complexes of lower energy present O–H···O (1Hyp-E amd 4Hyp-E) and N–H···O (2Hyp-E and 5Hyp-E) hydrogen bonds, which in many cases are accompanied by C–H···O interactions. Comparison of $BE_{CP,wat}$ values calculated for both EDOT···Ac-L-Hyp-NMe and EDOT···Ac-L-Pro-NMe complexes indicate that the interaction of the EDOT unit with Hyp is still more favored than with Pro in a very polar environment, as was also found in chloroform solution and in vacuum.

Hybrid QM/MM MD Calculations.

Figure 9 shows the averaged structures of both EDOT···Ac-L-Pro-NMe and EDOT···Ac-L-Hyp-NMe complexes from QM/MM-MD trajectories using chloroform and water as explicit solvent. The complex structure remained stable throughout the whole simulation regardless of solvent polarity. Comparison with the structures derived from QM calculations using implicit solvent (see previous subsection) reveals a very good agreement. All complexes are stabilized through convencitional and/or non-conventional hydrogen bonds in addition of van der Waals interactions between the five membered rings.

QM/MM-MD simulations show the same specific interaction for EDOT···Ac-L-Pro-NMe complexes in chloroform and water solutions (Figures 9a and 9b). This consists on a C–O···H interaction between the C=O group of the Ac blocking group and one hydrogen atom located at the dioxane ring of EDOT, which is identical to that obtained using implicit solvent solvent. As it can be seen, the O···H distance increases 0.22 Å with the solvent polarity while the distance between the centers of masses of the thiophene and pyrrolidine ring decreases by the same amount ($d_{r\text{-}r}$ in Table 5), evindencing an enhancement of the van der Waals interactions. On the

other hand, the QM/MM-MD trajectory on EDOT···Ac-L-Hyp-NMe in chloroform reveals three different types of specific interactions between the components (Figure 9c). These consist on two conventional hydrogen bonding interactions (*i.e.* N–H···O and O–H…O, where the hydrogen bonding donors are the N–H of NMe and O–H of Hyp while the hydrogen bonding acceptors are the oxygen atoms of dioxane ring) and a non-conventional C–O···H hydrogen bond involving the C=O of Ac and a hydrogen atom of the dioxane ring. Comparison with the results derived from PCM-MP2/6-31+G(d,p) calculations reveals that the QM/MM-MD description of EDOT···Ac-L-Pro-NMe complexes corresponds to the combination of 1Hyp-E and 2Hyp-E (Figure S2), which were found to be practically isoenergetic (Table 3).

The N–H···O hydrogen bond is the only of the three interactions detected in chloroform that remains in water (Figure 9d). This description is similar to that obtained for 5Hyp-E using an implicit water model (Figure S4), which is the lowest energy complex in water (Table 4). However, PCM calculations predicted an additional C–H···O interaction for 5Hyp-E that is not detected in Figure 9d. As occurred for EDOT···Ac-L-Pro-NMe, the distance between the five membered rings of each component is smaller in water than in chlofororm (Table 5), reflecting that the aggregation of hydrophobic moieties is promoted by the aqueous environment. However, this aggregation is notably smaller for EDOT···Ac-L-Pro-NMe than for EDOT···Ac-L-Hyp-NMe, which should be attributed to the hydrophilic hydroxyl group of Hyp. It is worth noting that the variation the $d_{r\text{-}r}$ distance with the polarity of the solvent observed in QM/MM-MD simulations was not detected in PCM-MP2/6-31+G(d,p) calculations (Tables 3 and 4), the latter methodology providing very similar $d_{r\text{-}r}$ values for the two solvents (*i.e.* $d_{r\text{-}r}$ values of ~3.78 and ~4.53 Å for EDOT···Ac-L-Pro-NMe and EDOT···Ac-L-Hyp-NMe, respectively).

Table 5 lists dihedral angles of Ac-L-Pro-NMe and Ac-L-Hyp-NMe averaged from QM/MM-MD trajectories on EDOT···Ac-L-Pro-NMe and EDOT···Ac-L-Hyp-NMe complexes in chloroform and water. As it can be seen, these values are very similar to those obtained using PCM-MP2/6-31+G(d,p) calculations (Tables 3 and 4). Thus, consideration of explicit solvent molecules only provokes a small reduction and increment of the dihedral angles ϕ and ξ, respectively.

Weak NCI between the two complex components, as well as between the complex components and the solvent, were analyzed by examining the reduced electron density gradient with the NCIPlot program.[66,67] This methodology allows an easy identification of the regions with strong and weak electron pairing. Figures 10 and 11 display the reduced density gradient isosurfaces of EDOT···Ac-L-Pro-NMe and EDOT···Ac-L-Hyp-NMe, respectively. The NCI analysis provides a very useful description of molecular interactions, which are frequently represented by an arbitrary color code: blue, green and red are used for highly attractive weak interactions (such as hydrogen bonds), extremely weak interactions (such as van der Waals) and repulsive interactions (such as steric clashes), respectively.

In EDOT···Ac-L-Pro-NMe complexes the two components are dominated by van der Waals interactions between the rings. The participation of these interactions in the stability of the complex is higher in water than in chloroform, as is evidenced by the isosurface extension (Figures 10a and 10b), which is also consistent the above discussed $d_{r\text{-}r}$ values. Interestingly, solvent-complex interactions are also dominated by non-specific van der Waals interactions in the two studied environments. However, the complex in water also shows small localized blue regions at the isosurfaces indicating the existence of specific hydrogen bonds, which are practically inexistent in chloroform, involving the peptide groups (Figures 10c and 10d). On the

other hand, inter-component NCI analyses on EDOT···Ac-L-Hyp-NMe complexes corroborate the previously discussed hydrogen bonds. Specifically, N–H···O, O–H···O and C–H···O interactions are clearly identified in the complex embedded in chloroform (blue zones at the isosurface displayed in Figures 11a) while in water only the N–H···O remains (Figure 11b). This behavior is provoked by formation of hydrogen bonds between the hydroxyl group of Hyp and explicit water molecules (Figure 11d).

CONCLUSIONS

Biocomposites made of PEDOT and collagen have been prepared by *in situ* anodic polymerization. Collagen affects the clustered morphology of PEDOT due to a phase separation that gives place to the apparition of micro- and submicrometric spherical-like aggregates of collagen rods. Although the electroactivity of PEDOT decreases upon the incorporation of collagen, the protein stabilizes the CP matrix as reveals the electrostability that is higher for P(EDOT:CLG) than for PEDOT. Cell viability assays indicates that the incorporation of collagen to PEDOT results in a drastic improvement of the bioactivity, in terms of cell adhesion, spreading and proliferation. Indeed, the biocomposite promotes the formation of 3D biostructures that resemble biological tissues.

QM and QM/MM-MD calculations on model complexes considering different environments have evidenced the importante of specific interactions, C–H···O non-conventional hydrogen bonds playing a crucial role. Results derived from methodologies that apply implicit and explicit solvation models are fully consistent, the interactions patterns described for all examined complexes being very similar independently of the solvent. Both energy gaps between the different calculated complexes and the binding energy decrease with increasing environmental

polarity. However, in all cases the interaction of EDOT with Hyp is stronger than with Pro. Finally, the different types of non-convalent interactions involved in the stabilization of the complexes (*i.e.* van der Waals and both conventional and non-conventional hydrogen bonds) have been clearly identified by visualizing the reduced electron density gradient.

SUPPORTING INFORMATION

Structures of EDOT···Ac-L-Pro-NMe and EDOT···Ac-L-Hyp-NMe optimized at the PCM-MP2/6-31+G(d,p) level in chloroform and water. This material is available free of charge via the Internet at http://pubs.acs.org.

ACKNOWLEDGEMENTS

This work was supported by MICINN-FEDER funds (MAT2012-34498) the Generalitat de Catalunya (2009SGR925 and XRQTC) and CESCA. J. S-D acknowledges support from Post-Doctoral fellow FONDECYT Grant 3130359 and Project ICM-P10-003-F CILIS granted by Fondo de Innovacion para la Competitividad del Ministerio de Economia, Fomento y Turismo, Chile.

REFERENCES

1. N. K. Guimard, N. Gomez and C. E. Schmidt, *Prog. Polym. Sci.*, 2007, **32**, 876−921.
2. H. C. Zhao, B. Zhu, S. C. Luo, H. A. Lin, A. Nakao, Y. Yamashita and H. H. Yu, *ACS Appl. Mater. Interfaces*, 2013, **5**, 4536−4543.
3. A.-D. Bendrea, G. Fabregat, L. Cianga, F. Estrany, L. J. del Valle, I. Cianga and C. Alemán, *Polym. Chem.*, 2013, **4**, 2709−2723.

4. A. Guiseppi-Elie, *Biomaterials*, 2010, **31**, 2701−2716.
5. M. M. Pérez-Madrigal, M. I. Giannotti, L. J. del Valle, L. Franco, E. Armelin, J. Puiggalí, F. Sanz and C. Alemán, *ACS Appl. Mater. Interfaces*, 2014, **6**, 2709−2723.
6. Z.Q. Shi, H. C. Gao, J. Feng, B. B. Ding, X. D. Cao, S. Kuga, Y. J. Wang, L. N. Zhang, J. Cai, *Angew. Chem. Int. Ed.*, 2014, **53**, 5380-5384.
7. E. Llorens, M. M. Pérez-Madrigal, E. Armelin, L. J. del Valle, J. Puiggalí and C. Alemán, *RSC Adv.*, 2014, **4**, 15245–15255.
8. J. G. Hardy, J. Y. Lee and C. E. Schmidt, *Curr. Opin. Biotechnol.*, 2013, **24**, 847−962.
9. A. B. Sanghvi, K. P.-H. Miller, A. M. Belcher and C. E. Schmidt, *Nat. Mater.*, 2005, **4**, 496−502.
10. G. Fabregat, B. Teixeira-Dias, L. J. del Valle, E. Armelin, F. Estrany and C. Alemán, *ACS Appl. Mater. Interfaces*, 2014, **6**, 11940−11954.
11. R. A. Green, N. H. Lovell and L. A. Poole-Warren, *Biomaterials*, 2009, **30**, 3637−3644
12. D. López-Pérez, D. Aradilla, L. J. del Valle and C. Alemán, *J. Phys. Chem. C*, 2013, **117**, 6607−6619.
13. K. Svennersten, M. Berggren, A. Richter-Dahlforsa, E. W. H. Jager, *Lab Chip.*, 2011, **11**, 3287−3293.
14. P. Jithendra, A. M. Rajam, T. Kalaivani, A. B. Mandal and C. Rose, *ACS Appl. Mater. Interfaces*, 2013, **5**, 7291-7298.
15. C. H. Jang, Y. B. Cho, M. G. Yeo and G. H. Kim, *Macromol. Biosci.*, 2013, **13**, 660-668.
16. Y. Cho and R. Ben Borgens, *J. Mater. Chem. B*, 2013, **1**, 4166-4170.
17. S. Z. Yow, C. H. Quek, E. K. F. Yim, C. T. Lim and K. W. Leong, *Biomaterials*, 2009, **30**, 1133-1142.

18. M. G. Yeo and G. H. Kim, *Chem. Mater.*, 2011, **24**, 903-913.

19. S.-Z. Yow, T. H. Lim, E. K. F. Yim, C. T. Lim and K. W. Leong, *Polymers*, 2011, **3**, 527-544.

20. B. Weng, X. Liu, R. Shepherd and G. G. Wallace, *Synth. Metals*, 2012, **162**, 1375-1380.

21. H.-S. Kim, H. L. Hobbs, L. Wang, M. J. Rutten and C. C. Wamser, *Synth. Metals*, 2009, **159**, 1313-1318.

22. M. Bongo, O. Winther-Jensen, S. Himmelberger, X. Strakosas, M. Ramuz, A. Hama, E. Stavrinidou, G. G. Malliaras, A. Salleo, B. Winther-Jensen and R. M. Owens, *J. Mater. Chem. B*, 2013, **1**, 3860-3867.

23. D. D. Ateh, P. Vadgama and H. A. Navsaria, *Tissue Eng.*, 2006, **12**, 645-655.

24. L. B. Groenendaal, F. Jonas, D. Freitag, H. Pielartzik and J. R. Reynolds, *Adv. Mater.*, 2000, **12**, 481-494.

25. S. Kirchmeyer and K. Reuter, *J. Mater. Chem.*, 2005, **15**, 2077-2088.

26. L. L. A. Pettersson, T. Johansson, F. Carlsson, H. Arwin and O. Inganas, *Synth. Met.*, 1999, **101**, 198-199.

27. B. L. Groenendaal, G. Zotti, P. H. Aubert, S. M. Waybright and J. R. Reynolds, *Adv. Mater.*, 2003, **15**, 855-879.

28. L. J. Del Valle, F. Estrany, E. Armelin, R. Oliver, and C. Alemán, *Macromol. Biosci.*, 2008, **8**, 1144–1151.

29. G. Fabregat, G. Ballano, E. Armelin, L. J. del Valle, C. Cativiela and C. Alemán, *Polym. Chem.*, 2013, **4**, 1412-1424.

30. G. Fabregat, G. Ballano, J. Casanovas, A. D. Laurent, E. Armelin, L.J. del Valle, C. Cativiela, D. Jacquemin and C. Alemán, *RSC Adv.* 2013, **3**, 21069-21083.

31. B. Teixeira-Dias, L.J. del Valle, D. Aradilla, F. Estrany and C. Alemán, *Macromol. Mater. Eng.*, 2012, **297**, 427-436.

32. Poater, J.; Casanovas, J.; Solà, M.; Alemán, C. *J. Phys. Chem. A* **2010,** *114,* 1023-1028.

33. C. Ocampo, R. Oliver, E. Armelin, C. Alemán and F. Estrany, *J. Polym. Res.*, 2006, **13**, 193.

34. J. Bachl, D. Zanuy, D. López-Pérez, G. Revilla-López, C. Alemán and D. Díaz-Díaz, *Adv. Funct. Mater.,* 2014, **24**, 4893–4904.

35. B. Teixeira-Dias, D. Zanuy, J. Poater, M. Solà, F. Estrany, L. J. del Valle and C. Alemán, *Soft* Matter, 2011, **7**, 9922-9932.

36. C. Alemán, B. Teixeira-Dias, D. Zanuy, F. Estrany, E. Armelin and L. J. del Valle, *Polymer*, 2009, **50**, 1965-1974.

37. D. Aradilla, F. Estrany and C. Alemán, *J. Appl. Polym. Sci.*, **2011**, *121*, 1982-1991.

38. J. Torras, J. Casanovas and C. Alemán, *J. Phys. Chem. A*, 2012, **116**, 7571-7583.

39. J. Casanovas and C. Aleman, *J. Phys. Chem. C*, 2007, **111**, 4823-4830.

40. M. J. Frisch, G. W. Trucks, H. B. Schlegel, G. E. Scuseria, M. A. Robb, J. R. Cheeseman, G. Scalmani, V. Barone, B. Mennucci, G. A. Petersson, H. Nakatsuji, M. Caricato, X. Li, H. P. Hratchian, A. F. Izmaylov, J. Bloino, G. Zheng, J. L. Sonnenberg, M. Hada, M. Ehara, K. Toyota, R. Fukuda, J. Hasegawa, M. Ishida, T. Nakajima, Y. Honda, O. Kitao, H. Nakai, T. Vreven, J. A. Jr Montgomery, J. E. Peralta, F. Ogliaro, M. Bearpark, J. J. Heyd, E. Brothers, K. N. Kudin, V. N. Staroverov, R. Kobayashi, J. Normand, K. Raghavachari, A. Rendell, J. C. Burant, S. S. Iyengar, J. Tomasi, M. Cossi, N. Rega, J. M. Millam, M. Klene, J. E. Knox, J. B. Cross, V. Bakken, C. Adamo, J. Jaramillo, R. Gomperts, R. E. Stratmann, O. Yazyev, A. J. Austin, R. Cammi, C. Pomelli, J. W.

Ochterski, R. L. Martin, K. Morokuma, V. G. Zakrzewski, G. A. Voth, P. Salvador, J. J. Dannenberg, S. Dapprich, A. D. Daniels, O. Farkas, J. B. Foresman, J. V. Ortiz, J. Cioslowski and D. J. Fox, *Gaussian 09, revision A.01*, Gaussian, Inc.: Wallingford, CT, 2009.

41. C. Møller and M. S. Plesset, *Phys. Rev.*, 1934, **46**, 618.
42. P. C. Hariharan and J. A. Pople, *Theor. Chim. Acta*, 1973, **28**, 213-222.
43. A. D. McLean and G. S. Chandler, *J. Chem. Phys.*, 1980, **72**, 5639-5648.
44. J. K. Rainey and M. C. Goh, *Protein Sci.*, 2002, **11**, 2748-2754.
45. S. F. Boys and F. Bernardi, *Mol. Phys.*, 1970, **19**, 553-566.
46. S. Miertus, E. Scrocco and J. Tomasi, *Chem. Phys.*, 1981, **55**, 117-129.
47. S. Miertus and J. Tomasi, *Chem. Phys.*, 1982, **65**, 239-245.
48. A. Perczel, J. G. Angyan, M. Kajtar, W. Viviani, J. L. Rivail, J. F. Marcoccia and I. G. Csizmadia, *J. Am. Chem. Soc.*, 1991, **113**, 6256-6265
49. A. Flores-Ortega, J. Casanovas, D. Zanuy, R. Nussinov and C. Alemán, *J. Phys. Chem. B*, 2007, **111**, 5475-5482.
50. A. Flores-Ortega, A. I. Jiménez, C. Cativiela, R. Nussinov, C. Alemán and J. Casanovas, *J. Org. Chem.*, 2008, **73**, 3418-3427.
51. A. Flores-Ortega, J. Casanovas, X. Assfeld and C. Alemán, *J. Org. Chem.*, 2009, **74**, 3101-3108.
52. P. Cieplak, J. Caldwell and P. Kollman, *J. Comput. Chem.*, 2001, **22**, 1048-1057.
53. W. L. Jorgensen, J. Chandrasekhar, J. D. Madura, R. W. Impey and M. L. Klein, *J. Chem. Phys.*, 1983, **79**, 926-935.

54. J. Wang, R. M. Wolf, J. W. Caldwell, P. A. Kollman and D. A. Case, *J. Comput. Chem.*, 2004, **25**, 1157-1174.

55. J. Preat, D. Zanuy, E. A. Perpète and C. Alemán, *Biomacromolecules*, 2011, **12**, 1298-1304.

56. D. Zanuy and C. Alemán, *Soft Matter*, 2013, **9**, 11634-11644.

57. Case, D. A.; Darden, T. A.; T.E. Cheatham, I.; Simmerling, C. L.; Wang, J.; Duke, R. E.; Luo, R.; Walker, R. C.; Zhang, W.; Merz, K. M., et al. *AMBER 12*, (2012) University of California, San Francisco.

58. J.-P. Ryckaert, G. Ciccotti and H. J. C. Berendsen, *J. Comput. Phys.*, 1977, **23**, 327-341.

59. A. Toukmaji, C. Sagui, J. Board and T. Darden, *J. Chem. Phys.*, 2000, **113**, 10913-10927.

60. J. Torras, E. Deumens and S. B. Trickey, *J. Comput. Aided Mater. Des.*, 2006, **13**, 201-212.

61. J. Torras, G. d. M. Seabra, E. Deumens, S. B. Trickey and A. E. Roitberg, *J. Comput. Chem.*, 2008, **29**, 1564-1573.

62. M. Valiev, E. J. Bylaska, N. Govind, K. Kowalski, T. P. Straatsma, H. J. J. Van Dam, D. Wang, J. Nieplocha, E. Apra, T. L. Windus and W. A. de Jong, *Comput. Phys. Commun.*, 2010, **181**, 1477-1489.

63. J. G. Warren, G. Revilla-López, C. Alemán, A. I. Jiménez, C. Cativiela and J. Torras, *J. Phys. Chem. B*, 2010, **114**, 11761-11770.

64. Y. Zhao and D. Truhlar, *Theor. Chem. Acc.*, 2008, **120**, 215-241.

65. E. G. Hohenstein, S. T. Chill and C. D. Sherrill, *J. Chem. Theory Comput.*, 2008, **4**, 1996-2000.

66. E. R. Johnson, S. Keinan, P. Mori-Sánchez, J. Contreras-García, A. J. Cohen and W. Yang, *J. Am. Chem. Soc.*, 2010, **132**, 6498-6506.

67. J. Contreras-García, E. R. Johnson, S. Keinan, R. Chaudret, J.-P. Piquemal, D. N. Beratan and W. Yang, *J. Chem. Theory Comput.*, 2011, **7**, 625-632.

68. D. Fang, R. Chaudret, J.-P. Piquemal and G. A. Cisneros, *J. Chem. Theory Comput.*, 2013, **9**, 2156-2160.

69. S. Krimm and J. Bendekar, *Adv. Protein Chem.*, 1986, **38**, 181.

70. H. Susi and D. M. Byler, *Methods Enzymol.*, 1986, **130**, 290.

71. P. Jithendra, A. M. Rajam, T. Kalaivani, A. M. Mandal and C. Rose, *ACS Appl. Mater. Interfaces*, 2013, **5**, 7291−7298.

72. O. S. Rabotyagova, P. Cebe and D. L. Kaplan, *Materials Science and Engineering: C*, 2008, **28**, 1420-1429.

73. M.A. Piza, C.J.L. Constantino, E.C. Venancio and L.H.C. Mattoso, *Polymer*, 2003, **44**, 5663–5670.

74. R. Improta, F. Mele, O. Crescenzi, C. Benzi and V. Barone, *J. Am. Chem. Soc.*, 2002, **124**, 7857-7865.

75. N. Panasik, E. S. Eberhardt, A. S. Edison, D. R. Powell and R. T. Raines, *Int. J. Pept. Protein Res.*, 1994, **44**, 262-269.

76. J. A. Hodges and R. T. Raines, *J. Am. Chem. Soc.*, 2003, **125**, 9262-9263.

77. E. S. Eberhardt, N. Panasik and R. T. Raines, *J. Am. Chem. Soc.*, 1996, **118**, 12261-12266.

78. R. Improta, C. Benzi and V. Barone, *J. Am. Chem. Soc.*, 2001, **123**, 12568-12577.

79. S. S. Zade and M. Bendikov, *J. Phys. Chem. C*, 2007, **111**, 10662-10672.

80. G. Fabregat, E. Córdova-Mateo, E. Armelin, O. Bertran and C. Alemán, *J. Phys. Chem. C*, 2011, **115**, 14933-14941.

CAPTIONS TO FIGURES

Figure 1. Chemical structure and dihedral angles of Ac-L-Pro-NHMe and Ac-L-Hyp-NHMe. The dihedral angles ω_0, ϕ, ψ, and ω are defined by using backbone atoms, while the endocyclic dihedral angles χ^i are given by the five-membered ring atoms. In particular, ϕ, χ^0, and ξ are defined by C(O)–N–C^{α}–C(O), C^{δ}–N–C^{α}–C^{β}, and N–C^{δ}–C^{γ}–O, respectively. The oxygen atom used to define ξ refers to the hydroxyl group of Hyp.

Figure 2. FTIR spectra in the 1730-1450 cm^{-1} range of free collagen, PEDOT and 4.5-P(EDOT:CLG) at room temperature.

Figure 3. SEM micrographs of: (a) PEDOT, (b) 18-P(EDOT:CLG) and (c) 4.5-P(EDOT:CLG). The scale bar corresponds to 1 μm in all cases.

Figure 4. Cyclic voltammograms of (a) PEDOT and (b) 4.5-P(EDOT:CLG) as prepared (black lines) and after 15 consecutive oxidation-reduction cycles (grey lines).

Figure 5. Cellular adhesión (a) and cellular proliferation (b) on PEDOT, 18-P(EDOT:CLG) and 4.5-P(EDOT:CLG). The relative viability of HEp-2 and Du-145 cells was established in relation to TCPS control (tissue culture polystyrene). Results are normalized per area of material.

Figure 6. SEM micrographs of HEp-2 cells cultured for 2 days on the surface of (a) PEDOT and (b) 4.5-P(EDOT:CLG). The domains with cells are marked with an asterisk within a black box while the connections or interactions between the cell and the surface are indicated in by arrows. (c) Formation of a cellular monolayer on the surface 4.5-P(EDOT:CLG) after 7 cultured days. (d) Adhesion of cells onto the first cellular monolayer to facilitate the formation of 3D biostructures made of superposed cell monolayers (e and f), mimicking the growing of biological tissues.

Figure 7. Representative EDOT···Ac-L-Pro-NMe complexes (*i.e.* relative energies ≤ 3 kcal/mol) optimized at the MP2/6-31+G(d, p) level in vacuum. Structural parameters and relative energies are provided in Table 2.

Figure 8. Representative of the EDOT···Ac-L-Hyp-NMe complexes (*i.e.* relative energies ≤ 3 kcal/mol) optimized at the MP2/6-31+G(d, p) level in vacuum. Structural parameters and relative energies are provided in Table 2.

Figure 9. Time-averaged structures of EDOT···Ac-L-Pro-NMe complex in (a) chloroform and (b) water solvent, and EDOT···Ac-L-Hyp-NMe complex in (c) chloroform and (d) water solvent. Hydrogen bond distances and angles with their corresponding standard deviations are shown. Calculation of the time-averaged structures was appropriated because of the low root mean square deviations obtained from the QM/MM-MD trajectories (see Methods section).

Figure 10. Weak non-covalent interactions obtained for the time-averaged structure EDOT···Ac-L-Pro-NMe: Intermolecular interactions in (a) chloroform and (b) water; and solute-solvent interactions in (c) chloroform and (d) water. Blue and green colors at the isosurfaces represent highly attractive weak interactions (such as hydrogen bonds) and extremely weak interactions (van der Waals), respectively. Calculation of the time-averaged structures was appropriated because of the low root mean square deviations obtained from the QM/MM-MD trajectories (see Methods section).

Figure 11. Weak non-covalent interactions obtained for the time-averaged structure EDOT···Ac-L-Hyp-NMe: Intermolecular interactions in (a) chloroform and (b) water; and solute-solvent interactions in (c) chloroform and (d) water. Blue and green colors at the isosurfaces represent highly attractive weak interactions (such as hydrogen bonds) and extremely weak interactions (van der Waals), respectively. Calculation of the time-averaged structures was

appropriated because of the low root mean square deviations obtained from the QM/MM-MD trajectories (see Methods section).

Table 1. Backbone Dihedral Angles (ϕ and ψ), Hydroxyl Moiety Diedral Angle (ξ), Pseudorotational Parameters (A and P) and Relative Energy (ΔE) for the Conformations of Ac-L-Pro-NHMe and Ac-L-Hyp-NHMe Optimized at the MP2/6-31+G(d,p) Level in Vacuum, Chloroform and Water.

	#Conf	ϕ (º)	ψ (º)[a]	ξ (º)[b]	(A, P) (º, º)	ΔE (kcal/mol)
			Vacuum			
Ac-L-Hyp-NHMe	ε_L[u]	-61.2	152.0	76.3	(39.5, 93.1)	0.0[c]
	ε_L[d]	-63.3	152.0	145.9	(38.3, -115.4)	< 0.1
Ac-L-Pro-NHMe	ε_L[d]	-66.8	163.0	148.1	(39.2,-121.5)	0.0[d]
	ε_L[u]	-61.1	163.0	78.5	(40.2, 105.5)	1.0
			Chloroform			
Ac-L-Hyp-NHMe	ε_L[u]	-63.4	152.0	76.9	(40.0, 87.4)	0.0[e]
	ε_L[d]	-66.5	152.0	148.5	(38.4, -109.5)	1.0
Ac-L-Pro-NHMe	ε_L[d]	-70.4	163.0	150.8	(39.3, -115.0)	0.0[f]
	ε_L[u]	-64.7	163.0	79.5	(39.9, 94.5)	0.6
			Water			
Ac-L-Hyp-NHMe	ε_L[u]	-63.8	152.0	77.1	(40.1, 86.1)	0.0[g]
	ε_L[d]	-66.9	152.0	150.0	(38.5, -105.8)	1.5
Ac-L-Pro-NHMe	ε_L[d]	-71.5	163.0	152.0	(39.3, -111.7)	0.0[h]
	ε_L[u]	-65.7	163.0	79.9	(39.9, 90.9)	0.4

[a] The dihedral angle ψ was constrained at 163º and 152º for Ac-L-Pro-NHMe and Ac-L-Hyp-NHMe, respectively. [b] The dihedral angle ξ (Figure 1) is defined by the sequence N-C^{δ}-C^{γ}-H^{γ} and N-C^{δ}-C^{γ}-O^{γ} for Ac-L-Pro-NHMe and Ac-L-Hyp-NHMe, respectively. [c] E = -646.653610 a.u. [d] E = -571.613048 a.u. [e] E = -646.669165 a.u. [f] E = -571.624794 a.u. [g] E = -646.676773 a.u. ; [h] E = -571.630847 a.u.

Table 2. Structural Information, Relative Energy (ΔE_{vac}) and Binding Energy ($BE_{CP,vac}$) for the EDOT···Ac-L-Pro-NHMe and EDOT···Ac-L-Hyp-NHMe Complexes Optimized at the MP2/6-31+G(d,p) Level in Vacuum.

Complex	#Conf	ϕ (º)	ψ (º)[a]	ξ (º)[b]	(A, P) (º, º)	d_{r-r} [c] (Å)	ΔE_{vac} (kcal/mol)	$BE_{CP,vac}$ [d] (kcal/mol)
				EDOT···Ac-L-Pro-NMe				
1Pro-E	ε_L[d]	-66.3	163.0	149.4	(38.8, -117.1)	3.775	0.0 [e]	-6.8
2Pro-E	ε_L[u]	-62.8	163.0	78.4	(40.3,99.7)	4.744	0.2	-8.1
3Pro-E	ε_L[d]	-66.4	163.0	148.5	(38.9,-120.1)	4.297	1.1	-6.0
4Pro-E	ε_L[d]	-73.2	163.0	157.6	(40.7,-98.6)	4.578	1.4	-6.8
5Pro-E	ε_L[u]	-57.6	163.0	79.7	(39.0,97.5)	3.879	1.7	-6.4
6Pro-E	ε_L[u]	-62.5	163.0	87.2	(40.6,65.8)	4.191	2.6	-6.2
7Pro-E	ε_L[u]	-70.9	163.0	80.2	(40.3,87.7)	5.464	2.8	-6.9
8Pro-E	ε_L[u]	-63.5	163.0	85.1	(40.3,87.7)	5.464	2.8	-6.7
9Pro-E	ε_L[u]	-67.0	163.0	79.6	(39.2,100.0)	3.720	3.0	-5.8
				EDOT···Ac-L-Hyp-NMe				
1Hyp-E	ε_L[u]	-55.1	152.0	79.5	(42.2,105.1)	4.833	0.0 [f]	-8.8
2Hyp-E	ε_L[u]	-63.6	152.0	77.0	(39.7,87.7)	4.673	1.2	-7.4
3Hyp-E	ε_L[d]	-65.6	152.0	153.2	(41.5,-95.4)	4.681	1.5	-8.4
4Hyp-E	ε_L[u]	-59.6	152.0	76.3	(40.3, 88.5)	4.746	2.3	-7.6
5Hyp-E	ε_L[u]	-55.8	152.0	78.0	(39.9, 81.3)	4.137	2.5	-6.6
6Hyp-E	ε_L[u]	-59.9	152.0	84.3	(41.6, 61.8)	4.191	2.6	-7.1
7Hyp-E	ε_L[u]	-54.6	152.0	75.3	(40.6, 88.3)	4.902	2.6	-7.4
8Hyp-E	ε_L[d]	-60.5	152.0	153.7	(41.1, -108.7)	4.734	2.7	-8.0
9Hyp-E	ε_L[d]	-62.4	152.0	141.6	(37.2, -122.9)	3.897	2.7	-6.1

[a] The dihedral angle ψ was constrained at 163º and 152º for Ac-L-Pro-NHMe and Ac-L-Hyp-NHMe, respectively. [b] The dihedral angle ξ (Figure 1) is defined by the sequence N-C^{δ}-C^{γ}-H^{γ} and N-C^{δ}-C^{γ}-O^{γ} for Ac-L-Pro-NHMe and Ac-L-Hyp-NHMe, respectively. [c] Distance between the centers of masses of the EDOT and pyrrolidine rings. [d] Calculated considering the CP correction. [e] E = -1350.841230 a.u. [f] E = -1425.885406 a.u.

Table 3. Structural Information, Relative Energy (ΔE_{chl}) and Binding Energy ($BE_{CP,chl}$) for the EDOT···Ac-L-Pro-NHMe and EDOT···Ac-L-Hyp-NHMe Complexes Optimized at the PCM-MP2/6-31+G(d,p) Level in Chloroform Solution.

Complex	#Conf	ϕ (º)	ψ (º)[a]	ξ (º)[b]	(A, P) (º, º)	d_{r-r} (Å) [c]	ΔE_{chl} (kcal/mol)	$BE_{CP,chl}$ [d] (kcal/mol)
				EDOT···Ac-L-Pro-NMe				
1Pro-E	ε_L[d]	-68.5	163.0	150.4	(38.8,-114.6)	3.781	0.0 [e]	-4.6
2Pro-E	ε_L[u]	-64.3	163.0	79.7	(40.2, 88.6)	4.466	1.4	-5.1
3Pro-E	ε_L[d]	-68.8	163.0	152.0	(39.0, -111.3)	4.273	1.2	-4.6
4Pro-E	ε_L[d]	-73.1	163.0	156.7	(40.4, -100.9)	4.539	1.5	-4.4
5Pro-E	ε_L[u]	-59.7	163.0	79.8	(39.2, 93.9)	3.926	0.5	-4.1
6Pro-E	ε_L[u]	-62.1	163.0	84.4	(40.3, 72.9)	4.243	2.3	-3.6
7Pro-E	ε_L[u]	-70.1	163.0	80.1	(40.4, 87.7)	5.453	2.8	-4.2
8Pro-E	ε_L[u]	-62.7	163.0	84.9	(38.3, 77.3)	4.315	2.8	-4.0
9Pro-E	ε_L[u]	-67.3	163.0	80.4	(39.0, 94.9)	3.731	1.4	-4.4
				EDOT···Ac-L-Hyp-NMe				
1Hyp-E	ε_L[u]	-55.1	152.0	80.6	(41.4, 100.3)	4.869	0.1	-5.8
2Hyp-E	ε_L[u]	-65.9	152.0	77.1	(39.2, 91.7)	4.525	0.0[c]	-5.2
3Hyp-E	ε_L[d]	-66.0	152.0	156.6	(41.7,-94.9)	4.667	1.7	-5.4
4Hyp-E	ε_L[u]	-59.6	152.0	77.6	(40.1,84.3)	4.775	0.1	-5.7
5Hyp-E	ε_L[u]	-59.0	152.0	79.0	(41.9,72.0)	4.474	0.3	-4.2
6Hyp-E	ε_L[u]	-59.3	152.0	82.5	(41.2,67.2)	4.204	2.0	-3.8
7Hyp-E	ε_L[u]	-53.3	152.0	75.3	(41.0,86.9)	4.612	1.5	-4.3
8Hyp-E	ε_L[d]	-62.9	152.0	153.4	(41.2,-108.8)	4.751	2.2	-5.4
9Hyp-E	ε_L[d]	-61.3	152.0	148.5	(38.3,-109.3)	3.894	1.0	-4.5

[a] The dihedral angle ψ was constrained at 163º and 152º for Ac-L-Pro-NHMe and Ac-L-Hyp-NHMe, respectively. [b] The dihedral angle ξ (Figure 1) is defined by the sequence N-C^{δ}-C^{γ}-H^{γ} and N-C^{δ}-C^{γ}-O^{γ} for Ac-L-Pro-NHMe and Ac-L-Hyp-NHMe, respectively. [c] Distance between the centers of masses of the EDOT and pyrrolidine rings. [d] Calculated considering the CP correction. [e] E = -1350.566316 a.u. [f] E = -1425.608341 a.u.

Table 4. Structural Information, Relative Energy (ΔE_{wat}) and Binding Energy ($BE_{CP,wat}$) for the EDOT···Ac-L-Pro-NHMe and EDOT···Ac-L-Hyp-NHMe Complexes Optimized at the PCM-MP2/6-31+G(d,p) Level in Water.

Complex	#Conf	ϕ (º)	ψ (º)[a]	ξ (º)[b]	(A, P) (º, º)	$d_{r\text{-}r}$ (Å)[c]	ΔE_{wat} (kcal/mol)	$BE_{CP,wat}$[d] (kcal/mol)
				EDOT···Ac-L-Pro-NMe				
1Pro-E	ε_L[d]	-68.8	163.0	151.2	(38.9, -112.6)	3.777	0.0[e]	-3.6
2Pro-E	ε_L[u]	-64.4	163.0	80.4	(40.4, 85.2)	4.394	0.7	-4.0
3Pro-E	ε_L[d]	-69.3	163.0	153.1	(39.1, -108.2)	4.311	0.6	-4.3
4Pro-E	ε_L[d]	-71.7	163.0	155.7	(40.0, -102.4)	4.517	1.5	-3.5
5Pro-E	ε_L[u]	-59.8	163.0	80.5	(39.4, 89.2)	3.930	1.5	-3.1
6Pro-E	ε_L[u]	-64.2	163.0	82.3	(40.5, 78.7)	4.344	2.0	-3.0
7Pro-E	ε_L[u]	-68.9	163.0	80.2	(40.4, 86.9)	5.433	3.0	-3.1
8Pro-E	ε_L[u]	-63.1	163.0	84.7	(38.3, 78.1)	4.312	2.3	-2.9
9Pro-E	ε_L[u]	-66.3	163.0	80.6	(39.3, 90.8)	3.754	0.7	-4.0
				EDOT···Ac-L-Hyp-NMe				
1Hyp-E	ε_L[u]	-55.2	152.0	81.4	(41.0, 96.2)	4.877	0.2	-4.7
2Hyp-E	ε_L[u]	-67.1	152.0	76.7	(39.7, 90.7)	4.678	0.3	-4.6
3Hyp-E	ε_L[d]	-65.5	152.0	156.9	(41.7, -93.9)	4.635	2.0	-4.0
4Hyp-E	ε_L[u]	-59.3	152.0	77.9	(40.2, 82.7)	4.786	0.1	-5.1
5Hyp-E	ε_L[u]	-62.2	152.0	77.7	(40.4, 81.5)	4.532	0.0[f]	-4.6
6Hyp-E	ε_L[u]	-63.0	152.0	79.1	(40.8, 77.0)	4.368	1.5	-3.2
7Hyp-E	ε_L[u]	-53.3	152.0	76.1	(40.7, 85.2)	4.616	0.8	-3.2
8Hyp-E	ε_L[d]	-64.9	152.0	153.5	(40.9, -109.8)	4.542	2.3	-4.3
9Hyp-E	ε_L[d]	-61.5	152.0	149.5	(38.4, -106.7)	3.877	2.8	-3.8

[a] The dihedral angle ψ was constrained at 163º and 152º for Ac-L-Pro-NHMe and Ac-L-Hyp-NHMe, respectively. [b] The dihedral angle ξ (Figure 1) is defined by the sequence N-C^{δ}-C^{γ}-H^{γ} and N-C^{δ}-C^{γ}-O^{γ} for Ac-L-Pro-NHMe and Ac-L-Hyp-NHMe, respectively. [c] Distance between the centers of masses of the EDOT and pyrrolidine rings. [d] Calculated considering the CP correction. [e] E = -1350.566316 a.u. [f] E = -1425.616442 a.u.

Table 5. Average Backbone Dihedral Angles (in deg) and Inter-ring Distance (d_{r-r}) Derived from the MD/MM-MDTrajectories in Explicit Solvent for EDOT···Ac-L-Pro-NHMe and EDOT···Ac-L-Hyp-NHMe Complexes s. Standard Deviations Are Shown.

Solvent	**#Conf**	**ϕ (º)**	**ψ (º)**	**ξ (º)[a]**	**d_{r-r} (Å)[b]**
		EDOT···Ac-L-Pro-NMe			
Chloroform	ε_L[d]	-57.9±6.9	162.9±0.5	155.2±8.9	4.20±0.09
Water	ε_L[d]	-68.5±6.2	163.0±0.4	153.1±7.4	3.98±0.14
		EDOT···Ac-L-Hyp-NMe			
Chloroform	ε_L[u]	-65.7±8.5	151.9±0.5	77.0±4.5	4.82±0.10
Water	ε_L[u]	-59.8±6.7	152.0±0.7	84.4±7.2	4.64±0.11

[a] The dihedral angle ξ (Figure 1) is defined by the sequence N-C^{δ}-C^{γ}-H^{γ} and N-C^{δ}-C^{γ}-O^{γ} for Ac-L-Pro-NHMe and Ac-L-Hyp-NHMe, respectively. [b] Distance between the centers of masses of the EDOT and pyrrolidine rings.

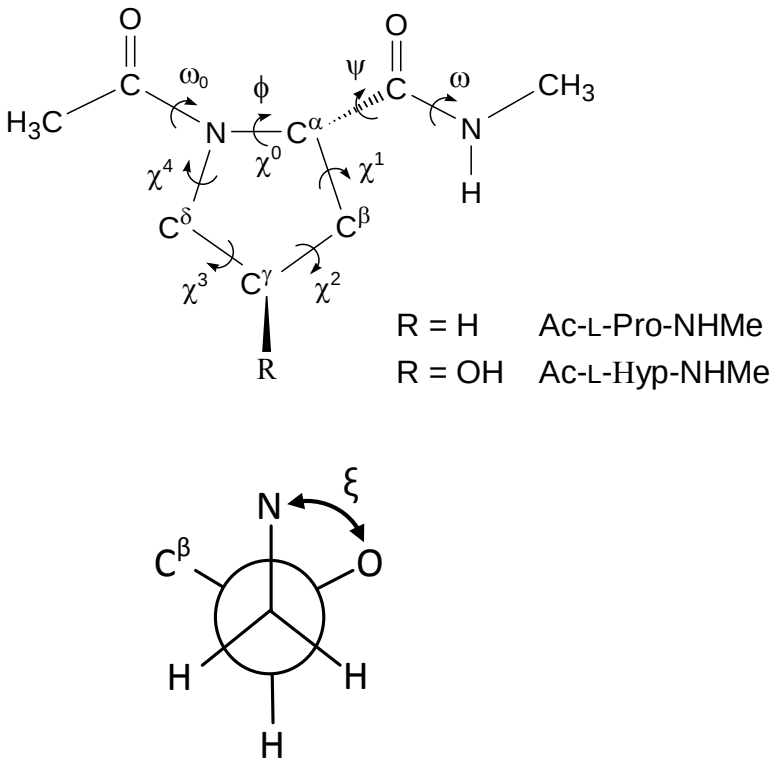
O
C
H3C
ω0
N
ϕ
Cα
ψ
O
C
ω
N
CH3
H
χ4
χ0
χ1
Cδ
Cβ
χ3
Cγ
χ2
R
R = H Ac-L-Pro-NHMe
R = OH Ac-L-Hyp-NHMe

N
ξ
Cβ
O
H
H
H

Figure 1

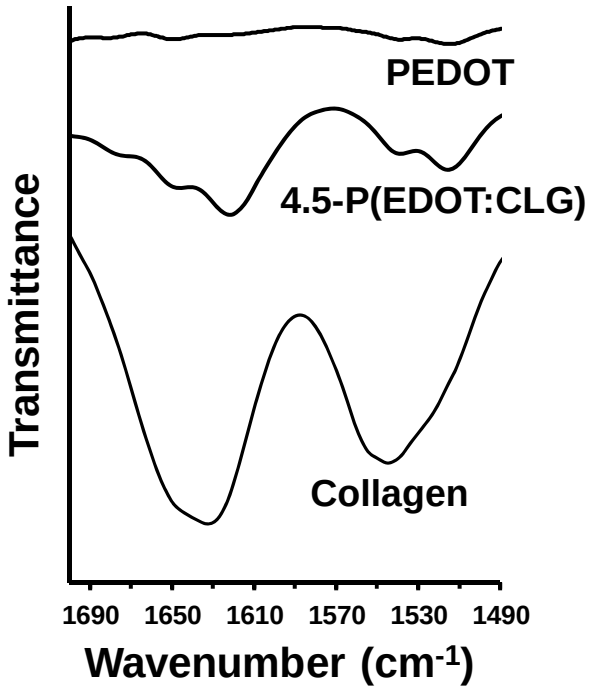
PEDOT
4.5-P(EDOT:CLG)
Collagen
Transmittance
1690
1650
1610
1570
1530
1490
Wavenumber (cm-1)

Figure 2

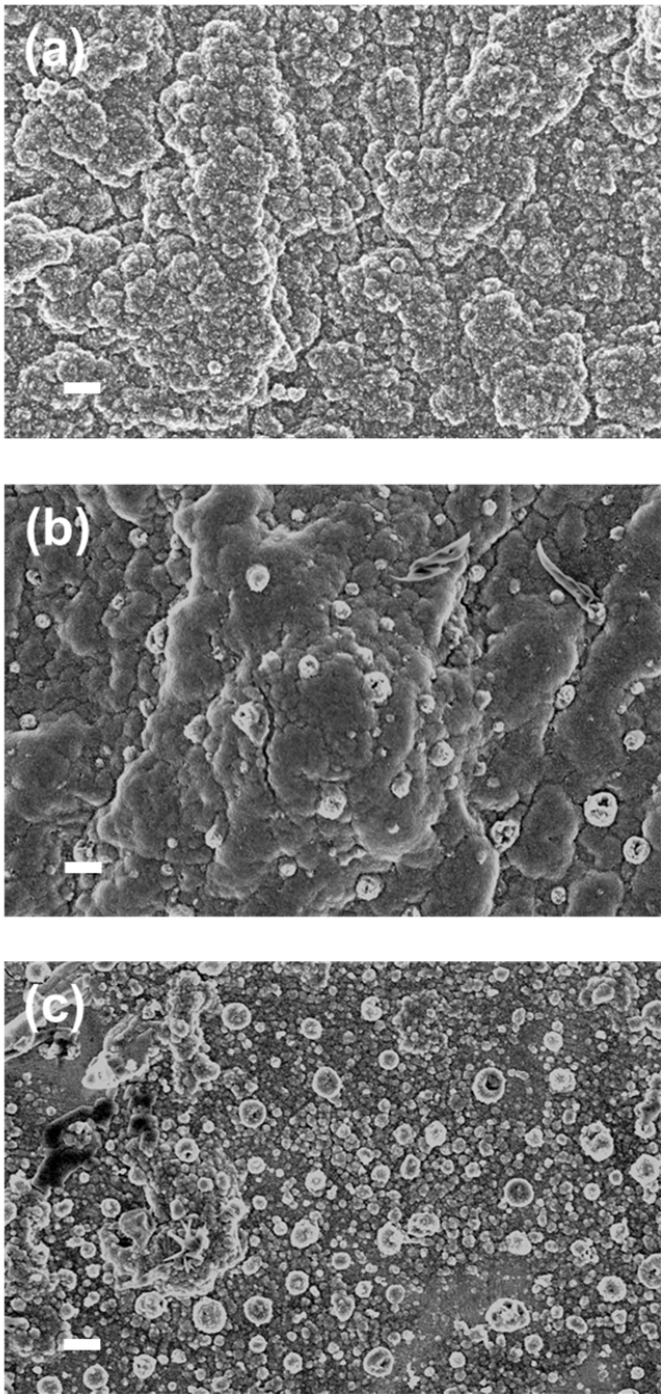

Figure 3

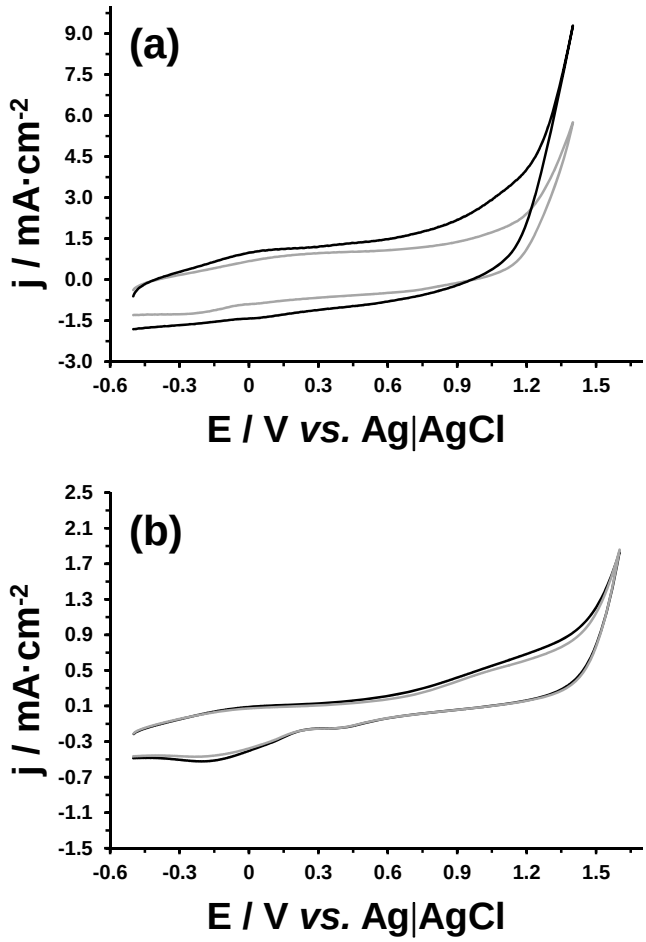
(a)
9.0
7.5
6.0
4.5
3.0
1.5
0.0
-1.5
-3.0
j / mA·cm-2
-0.6
-0.3
0
0.3
0.6
0.9
1.2
1.5
E / V vs. Ag|AgCl
(b)
2.5
2.1
1.7
1.3
0.9
0.5
0.1
-0.3
-0.7
-1.1
-1.5
j / mA·cm-2
-0.6
-0.3
0
0.3
0.6
0.9
1.2
1.5
E / V vs. Ag|AgCl

Figure 4

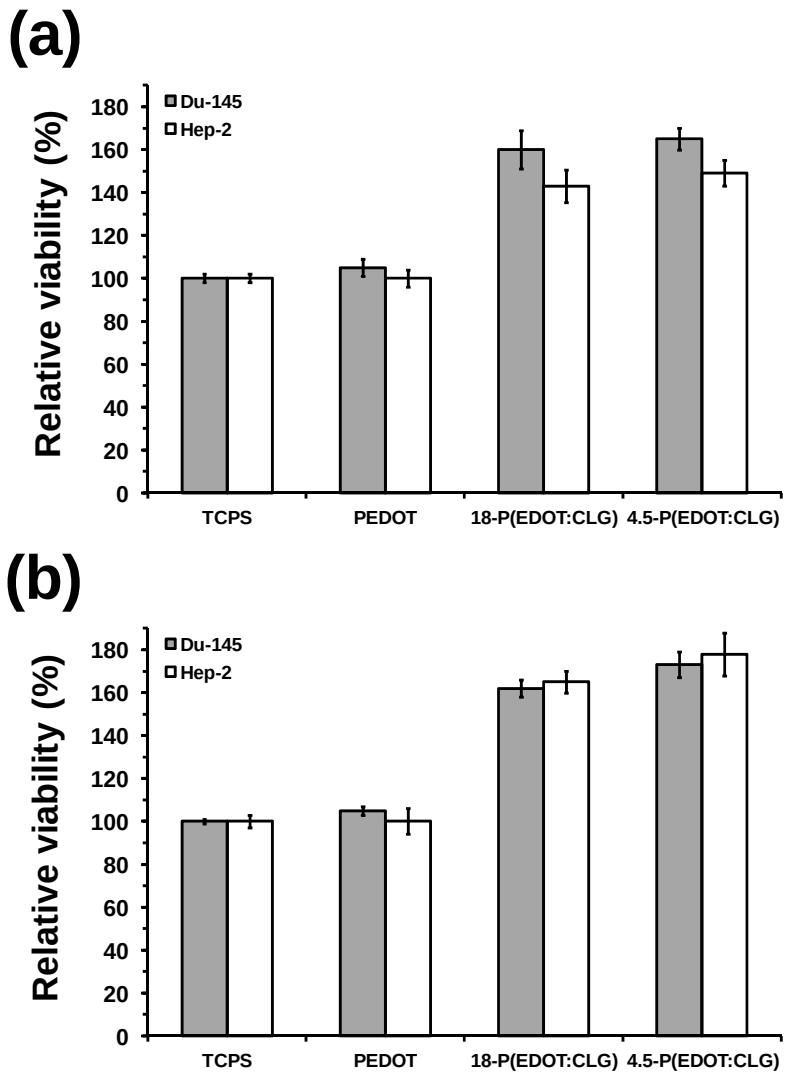
(a)
Relative viability (%)
Du-145
Hep-2
0
20
40
60
80
100
120
140
160
180
TCPS
PEDOT
18-P(EDOT:CLG)
4.5-P(EDOT:CLG)
(b)
Relative viability (%)
Du-145
Hep-2
0
20
40
60
80
100
120
140
160
180
TCPS
PEDOT
18-P(EDOT:CLG)
4.5-P(EDOT:CLG)

Figure 5

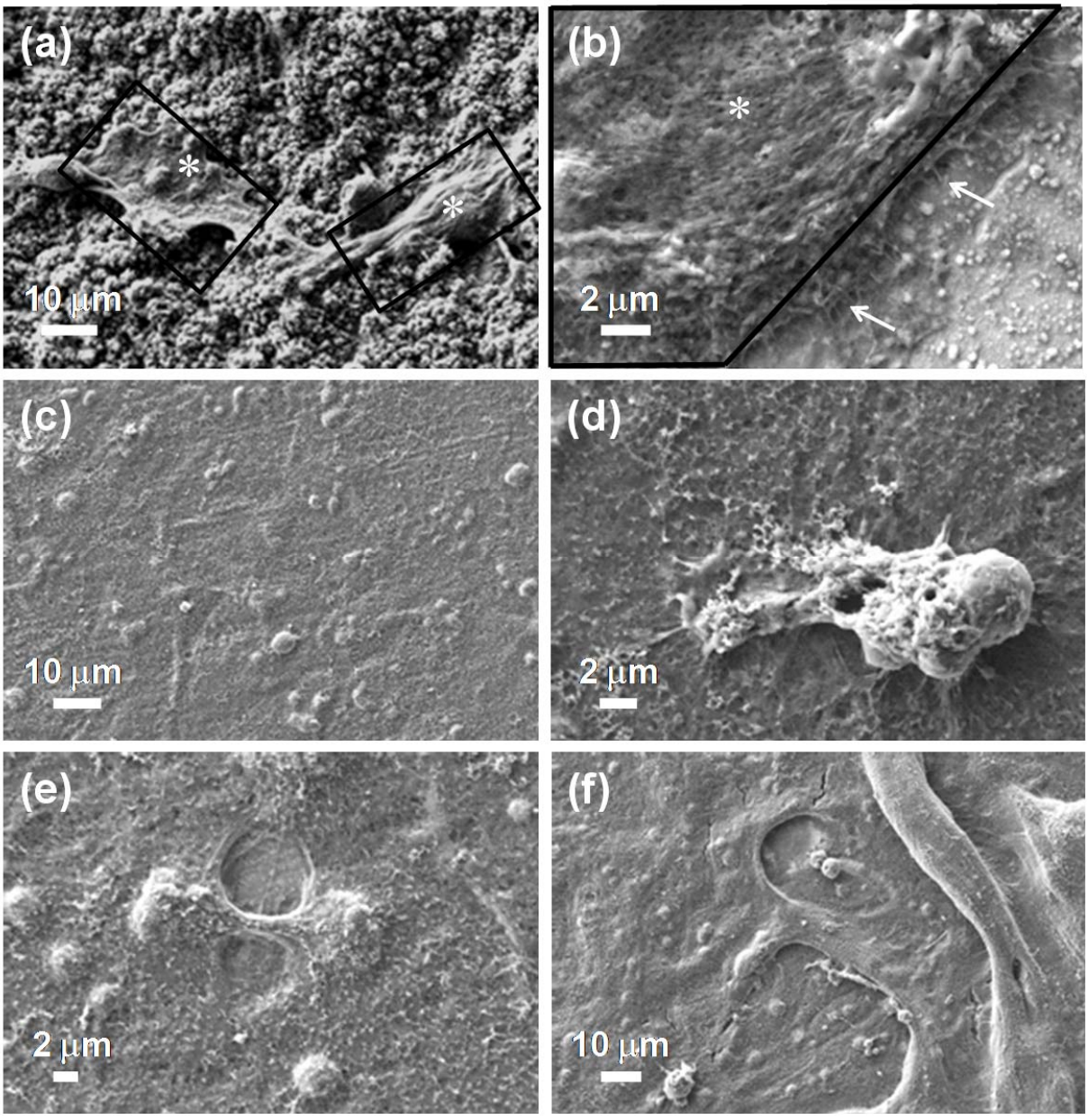

Figure 6

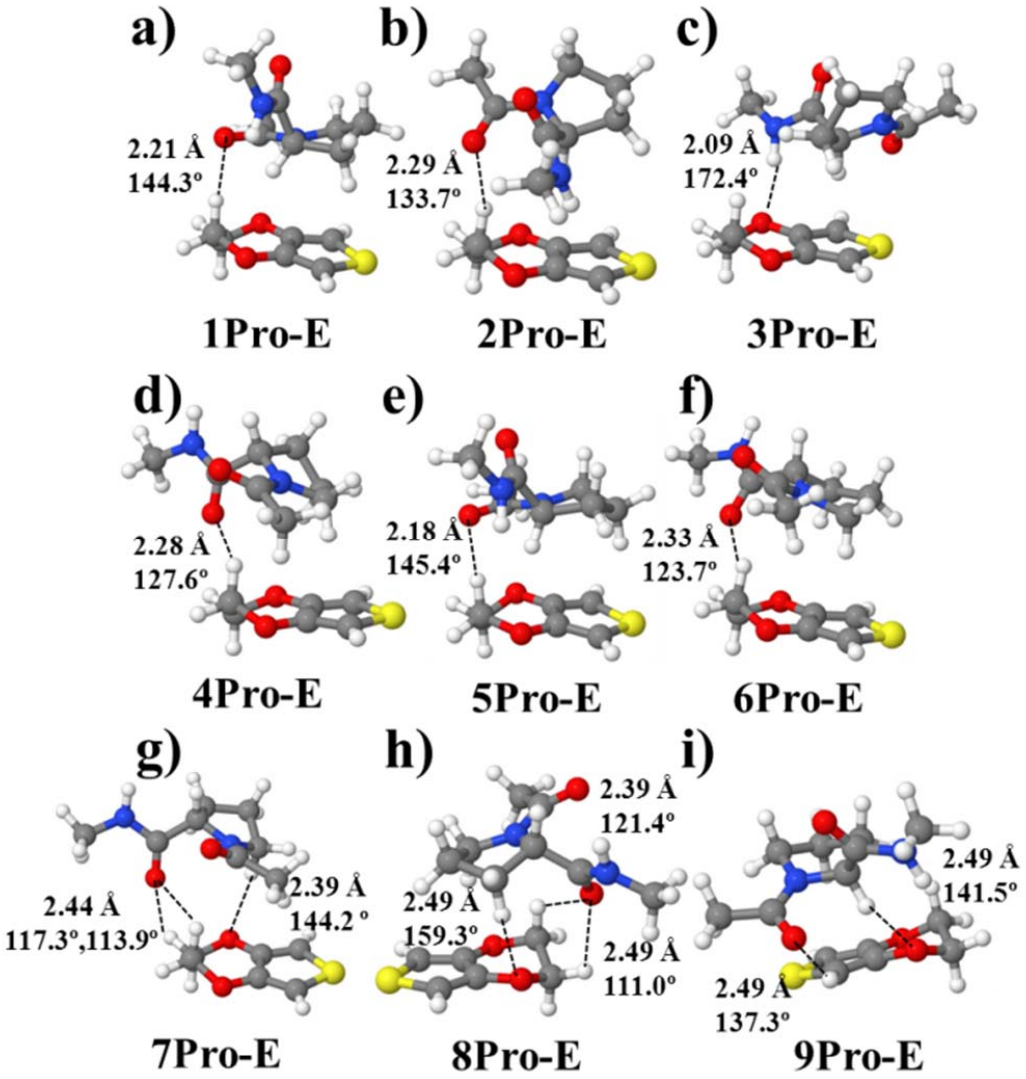
a)
2.21 Å
144.3°
1Pro-E
b)
2.29 Å
133.7°
2Pro-E
c)
2.09 Å
172.4°
3Pro-E
d)
2.28 Å
127.6°
4Pro-E
e)
2.18 Å
145.4°
5Pro-E
f)
2.33 Å
123.7°
6Pro-E
g)
2.44 Å
117.3°,113.9°
2.39 Å
144.2 °
7Pro-E
h)
2.39 Å
121.4°
2.49 Å
159.3°
2.49 Å
111.0°
8Pro-E
i)
2.49 Å
141.5°
2.49 Å
137.3°
9Pro-E

Figure 7

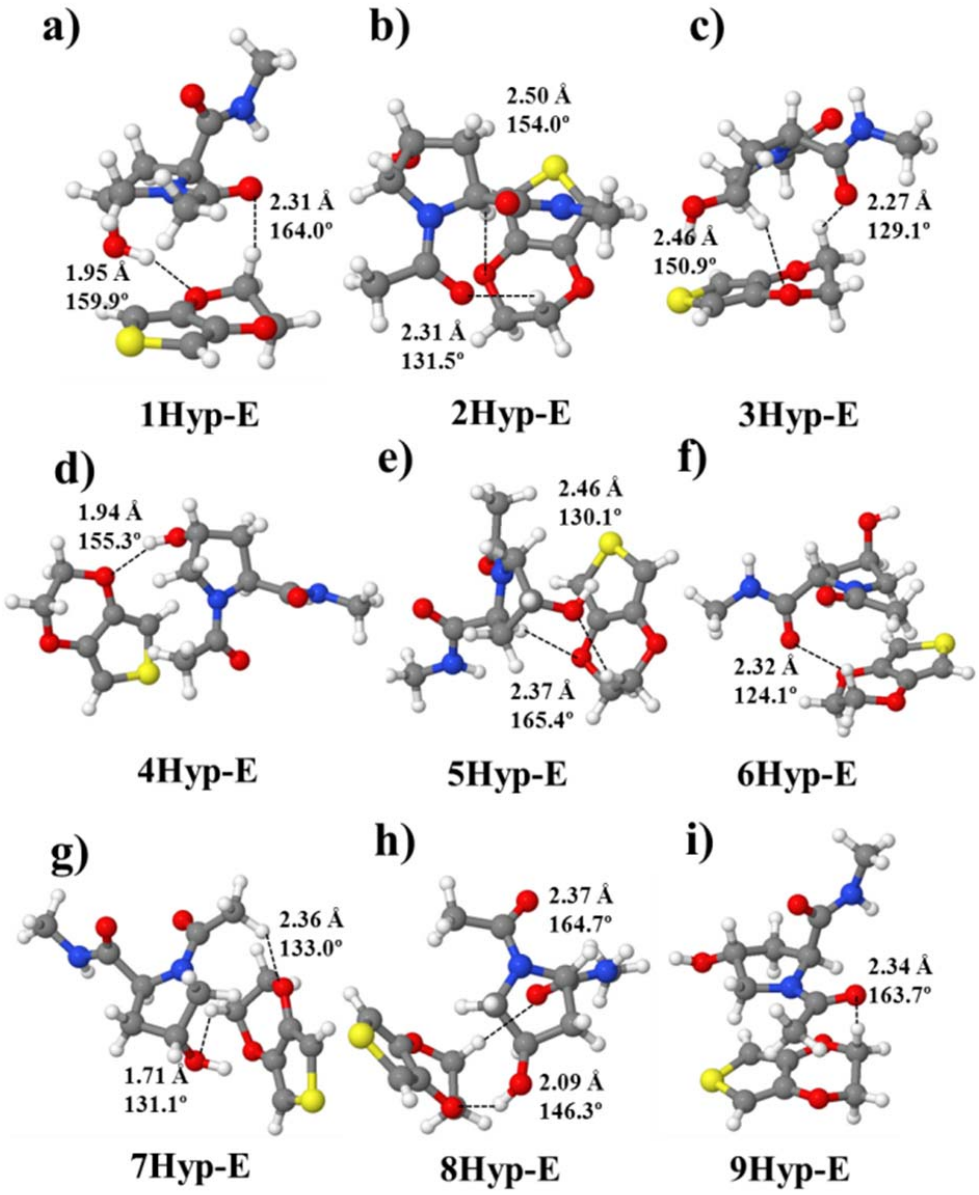
a)
2.31 Å
164.0°
1.95 Å
159.9°
1Hyp-E
b)
2.50 Å
154.0°
2.31 Å
131.5°
2Hyp-E
c)
2.27 Å
129.1°
2.46 Å
150.9°
3Hyp-E
d)
1.94 Å
155.3°
4Hyp-E
e)
2.46 Å
130.1°
2.37 Å
165.4°
5Hyp-E
f)
2.32 Å
124.1°
6Hyp-E
g)
2.36 Å
133.0°
1.71 Å
131.1°
7Hyp-E
h)
2.37 Å
164.7°
2.09 Å
146.3°
8Hyp-E
i)
2.34 Å
163.7°
9Hyp-E

Figure 8

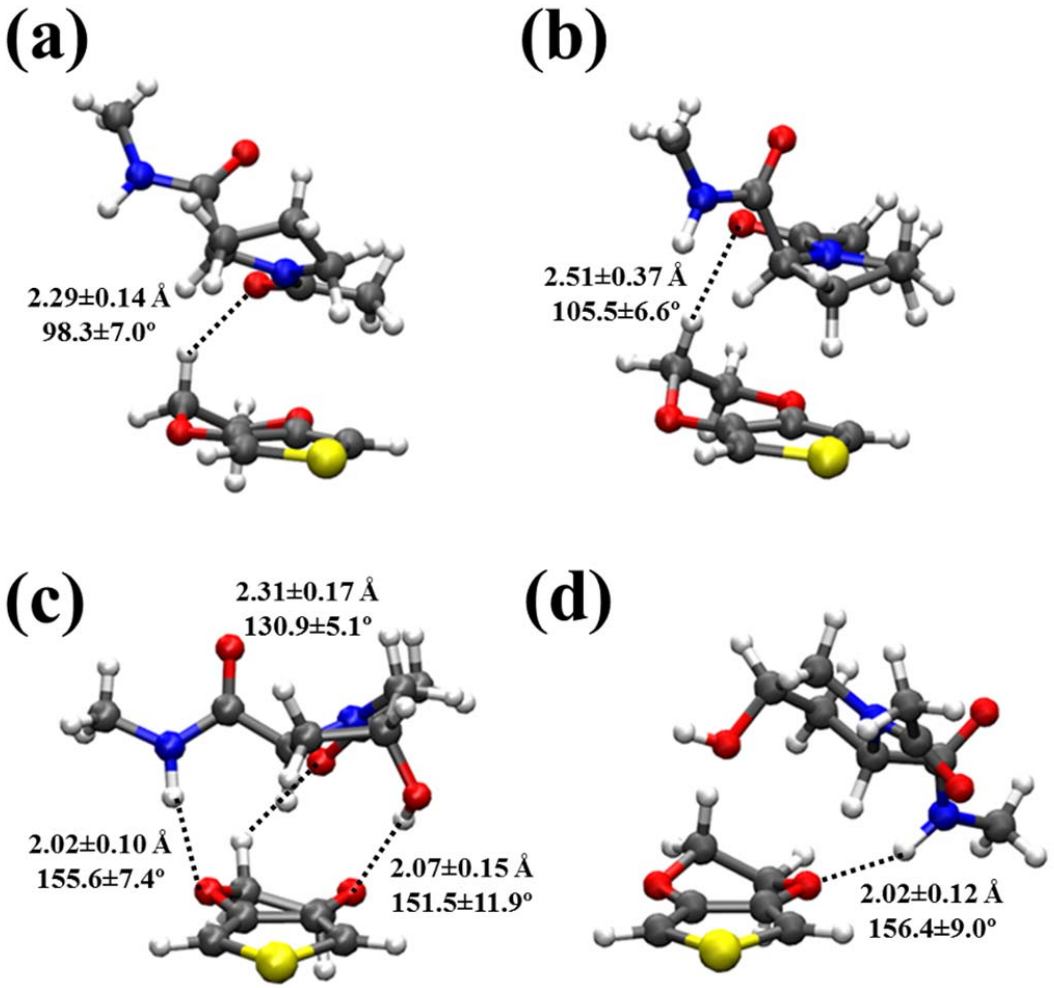
(a)
2.29±0.14 Å
98.3±7.0°
(b)
2.51±0.37 Å
105.5±6.6°
(c)
2.31±0.17 Å
130.9±5.1°
2.02±0.10 Å
155.6±7.4°
2.07±0.15 Å
151.5±11.9°
(d)
2.02±0.12 Å
156.4±9.0°

Figure 9

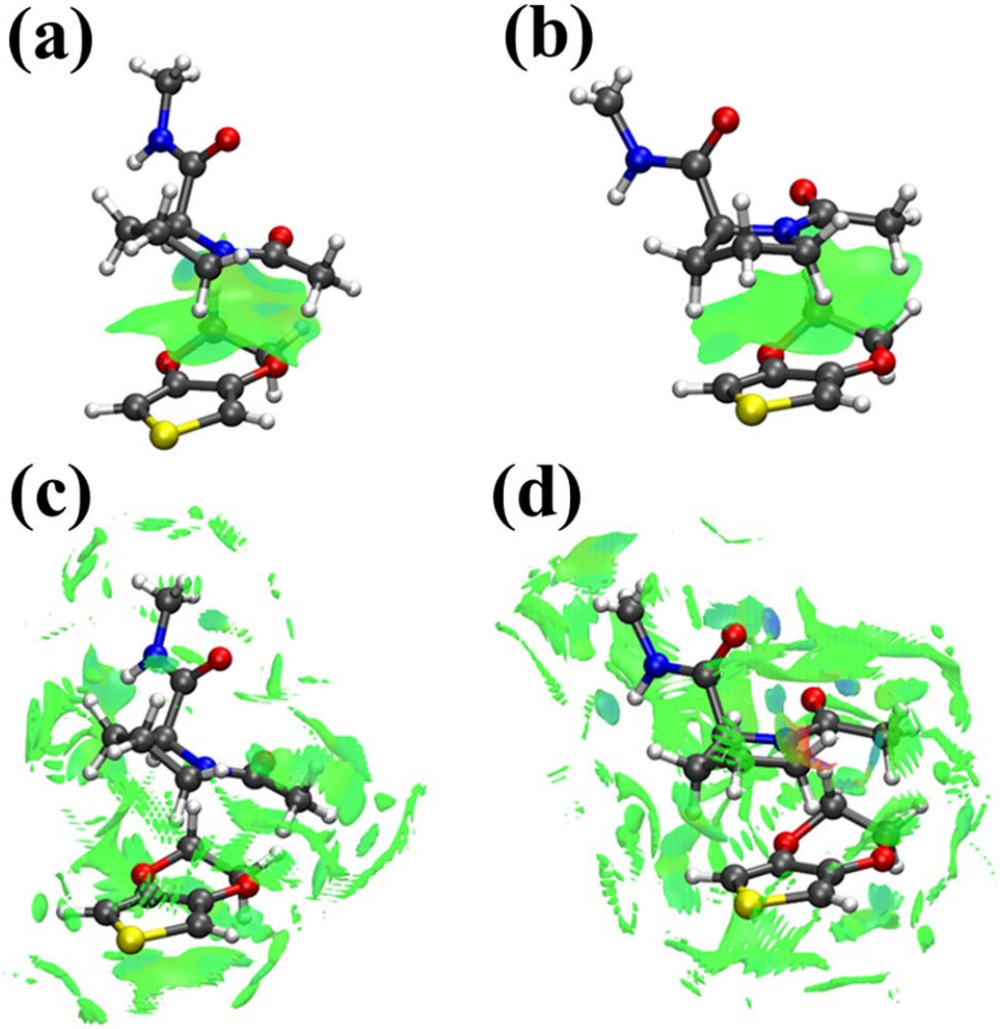

Figure 10

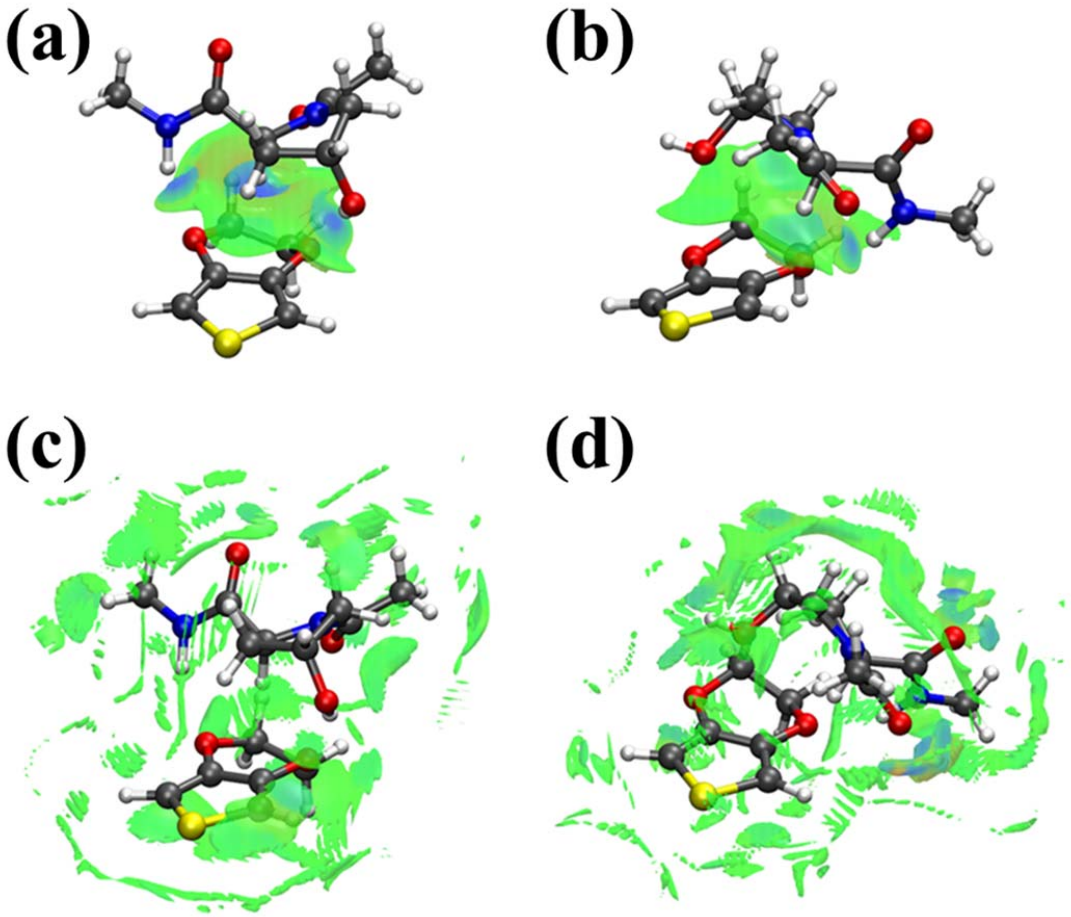

Figure 11

Graphical Abstract

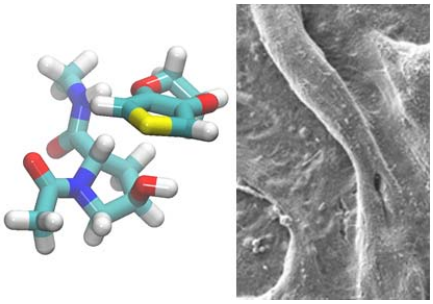

Poly(3,4-ethylenedioxythiophene) and collagen interact specifically forming biocomposites that mimic the growing of biological tissues